Available online at www.sciencedirect.com
SCIENCE DIRECT®
Journal of Sound and Vibration 280 (2005) 777–813
JOURNAL OF SOUND AND VIBRATION
www.elsevier.com/locate/jsvi

Shallow cavity flow tones: transformation from large- to small-scale modes

P. Oshkai[a], D. Rockwell[a,*], M. Pollack[b]

[a]*Department of Mechanical Engineering, and Mechanics, Lehigh University, 356 Packard Laboratory, 19 Memorial Drive West, Bethlehem, PA 18015-3085, USA*
[b]*Lockheed-Martin, P.O. Box 1072, Schenectady, NY 12301, USA*

Received 7 November 2002; accepted 17 December 2003
Available online 14 October 2004

Abstract

The generation of flow tones in an axisymmetric cavity is addressed for the case where the inflow is fully turbulent and the acoustic wavelength is much longer than the cavity length. Emphasis is on the nature of flow tones in relation to variations of cavity length. For a sufficiently long cavity, the fully evolved axisymmetric instability yields a large-scale mode. When the cavity length is decreased to progressively smaller values, the mode of oscillation transforms from the large-scale mode to a small-scale mode; it occurs at small values of cavity length, and scales on the momentum thickness of the separating shear layer. At a minimum value of cavity length, distinct oscillations do not occur. The existence of pronounced oscillations, i.e., flow tones, is also related to the dimensionless cavity depth. Oscillations are suppressed when the cavity depth is sufficiently small relative to the momentum thickness of the inflow boundary layer.

1. Introduction

1.1. Flow tone generation in various shear layer–resonator systems: an overview

The generation of flow tones, which involves compatibility between an inherent hydrodynamic instability of a separated shear layer and a resonant acoustic mode of the flow system, can occur

*Corresponding author. Tel.: +1-610-758-4107; fax: +1-610-758-4041.
E-mail address: dor0@lehigh.edu (D. Rockwell).

0022-460X/$ - see front matter
doi:10.1016/j.jsv.2003.12.054

in a wide variety of internal and external flow systems, as reviewed by Rockwell and Naudascher [1,2], Rockwell [3], Blake [4], Howe [5,6], Rockwell [7] and Rockwell et al. [8]. Representative configurations include jet excitation of a long organ pipe [9], a jet through a sequence of orifice plates [10,11], a shear flow past a cavity resonator [12–16]; and a shear layer past a resonant side branch in the form of a duct or pipe [17–22]. These flow tone configurations are described in further detail by Rockwell et al. [8].

Directly related to the present investigation are the tones arising from a shear layer past a cavity, which is located within a long pipeline, as addressed in a range of studies extending from Davies [23] to Davies [24,25]. Various physical features of the oscillation field within the cavity were characterized by Rockwell and Schachenmann [26,27] and Rockwell and Karadogan [28]. Conceptual issues related to this type of flow tone generation are described below. It is appropriate, however, to first address the hydrodynamic nature of cavity oscillations.

1.2. Hydrodynamics of the shear layer past a cavity: effect of cavity length

Oscillations of the shear flow past a cavity that arise from strictly hydrodynamic effects, in absence of acoustic resonance, show a number of fundamental features that may be inherent to the coupled oscillation of a shear layer and an acoustic resonator. Ethembabaoglu [29] demonstrated that the variation of dimensionless frequency with dimensionless cavity length, i.e., fL/U versus L/W, tended towards an asymptotic value for sufficiently large L/W, in which L is the cavity length, W represents the cavity depth, and U is the free-stream velocity. Oscillations were precluded at a sufficiently small value of L/W. Furthermore, a total of three oscillation modes, each having a pronounced spectral peak, existed over the range of L/W. Sarohia [30,31] determined the minimum dimensionless cavity length L_m for the onset of oscillations. This minimum length was expressed in terms of the cavity depth W normalized by the thickness δ_0 of the inflow boundary layer. Rockwell and Knisely [32] and Knisely and Rockwell [33] showed that variations of cavity length L resulted in generation of multiple peaks in the spectra of pressure fluctuations at the impingement corner and, moreover, that these multiple peaks were associated with processes of nonlinear interaction and deterministic mechanisms of vortex–corner interaction. Gharib and Roshko [34] revealed the importance of the length-to-depth ratio of the cavity in relation to a self-sustained oscillation mode and a wake mode of instability; furthermore, they related these modes to the mean drag. Howe [5] theoretically determined the variation of dimensionless frequency fL/U versus b/L, in which b is the spanwise width of the cavity. Favorable comparison was achieved with the experimental results of Ahuja and Mendoza [35].

1.3. Shear layer past a cavity coupled with long-wavelength acoustic resonance in a pipeline: effect of cavity length

The characteristics of strictly hydrodynamic oscillations of a shear layer past a cavity, which are described in the preceding section, may couple with, and be altered by, presence of acoustic resonance. More specifically, this coupling may involve a resonant mode having a characteristic acoustic wavelength λ_a much longer than the cavity length L, i.e., $L/\lambda_a \ll 1$. The present configuration is a cavity bounded by a pipe at its inlet and outlet. The resonant modes, which

occur in the entire system of the pipeline–cavity arrangement, satisfy the condition $L/\lambda_a \ll 1$. Since for all experiments described in the current article, the acoustic wavelength is much longer than the cavity dimension, it will not undergo resonance when facing an unbounded flow. Only the resonance of the pipeline–cavity system is therefore relevant.

For a generally similar configuration, Davies [23] characterized the relative sound level in relation to the effective length L of a cavity; he included the special case of a tailpipe protruding into the cavity. The sound pressure level generally decreased with increasing L. These studies included a range of Mach number M and modal frequencies, which provided a range of L/λ_a. Schachenmann and Rockwell [36] addressed the configuration of a pipe–cavity–orifice arrangement, i.e., only an inlet pipe was present. In these experiments, the condition $L/\lambda_a \ll 1$ was always satisfied. Both upward and downward jumps of the predominant oscillation (flow tone) frequency occurred with increasing cavity length L. Furthermore, a lower limit of L was defined; it corresponded to the cessation of oscillations. Stoubos et al. [11] investigated the generation of flow tones in a pipe with flow restrictors. Although they did not consider continuous variations of the effective length L between restrictors, they showed that it was possible to obtain different spectral peaks of the pressure fluctuation for discrete values of L.

The recent work of Rockwell et al. [8] addressed the case of an axisymmetric cavity with pipes of equal length at its inlet and outlet; they focused on a single, limiting case of long cavity length. Self-excited flow tones occurred in a large-scale mode, which corresponded to the fully evolved axisymmetric mode of the jet instability through the cavity. The present study examines the consequences of variation of the cavity length L. More specifically, emphasis is on the transformation from the limiting case of the large-scale mode to intermediate- and small-scale modes, which occur for decreasing values of cavity length L.

1.4. Flow tones in pipeline–cavity systems: unresolved issues

To date, a number of central issues have not been addressed for self-sustained oscillations of flow past a shallow cavity in presence of a long wavelength resonator. More specifically, variation of the cavity length L permits, in concept, generation of oscillations at long and short cavity lengths, corresponding respectively to large- and small-scale modes of the cavity oscillation. The unresolved issues are as follows:

(1) For the case of a fully turbulent inflow, it is known [8] that a large-scale mode can be generated at long cavity length. The possible generation of a small-scale mode, which may emerge above the background turbulence at short values of cavity length L, has not been addressed.
(2) The large-scale mode of cavity oscillation, which occurs at long cavity length L, scales on the diameter D of the inflow pipe. At the other extreme, corresponding to a small-scale mode at short length L, the appropriate length scale for normalization is likely to be the momentum thickness θ_0 of the separating shear layer. If so, scaling of the unstable frequency on the basis of inviscid instability for a thin shear layer should be pursued.
(3) As the cavity length L is varied, it is expected that the amplitude of the predominant pressure fluctuation will vary accordingly. This amplitude variation has not been characterized, despite its importance in understanding the nature of flow tone generation corresponding to the

transformation from large- to small-scale modes at relatively large and small cavity lengths, respectively. Rather, emphasis in previous investigations has been on variation of the predominant frequency(ies) with cavity length.

(4) At each value of cavity length L, the possibility of two or more coexisting modes of resonant flow tones should be addressed. For the corresponding case of purely hydrodynamic oscillations of a laminar inflow, it is known that multiple spectral components may be present. The possibility of coincidence of such spectral components with resonant modes of the pipeline–cavity system has not been examined.

(5) For a pipeline–cavity system, whereby pipes of equal length are located at the inlet and outlet of the cavity, it is known from a previous investigation [8] that flow tones can occur only for even numbered modes of the pipeline–cavity resonator. The effect of this even mode constraint on the possible coupling with the multiple spectral components of the unstable cavity shear layer (described in item (4)) has not been pursued. Presumably, this coupling would require that the increment of frequency between the multiple components of the shear layer is in accord with the increment between resonator models.

(6) At sufficiently shallow cavity depth W, it is anticipated that oscillations in both the large- and small-scale modes, as well as intermediate modes between them, will be attenuated. This limiting value of cavity depth, suitably normalized by inflow pipe diameter D or inflow boundary layer thickness θ_0, has not been addressed except for the limiting case of the large-scale mode at long cavity length.

The aim of this investigation is to pursue these issues with the aid of pressure measurements within the pipeline–cavity system, and to interpret them with three-dimensional representations of the pressure response, along with a technique for extracting the predominant components.

2. Experimental system and techniques

2.1. Overview of experimental system

The experimental system consisted of an air supply and conditioning unit, and the actual pipeline–cavity system, both of which are described in detail by Rockwell et al. [8]. Air was supplied from a compressor and passed through a drying apparatus in a storage tank. All of these components were located in a separate room from the main experimental apparatus in order to minimize undesirable noise and disturbances. Air from the storage tank was transmitted through a thick ceramic wall, then a system of pressure regulators, which maintained a constant downstream pressure, and thereby a highly consistent flow rate through the pipeline–cavity system.

2.2. Pipeline–cavity system

An overview of the pipeline–cavity system is given in Fig. 1a. The actual pipeline–cavity arrangement is located downstream of an inlet plenum. A length of pipe L_A was connected to the

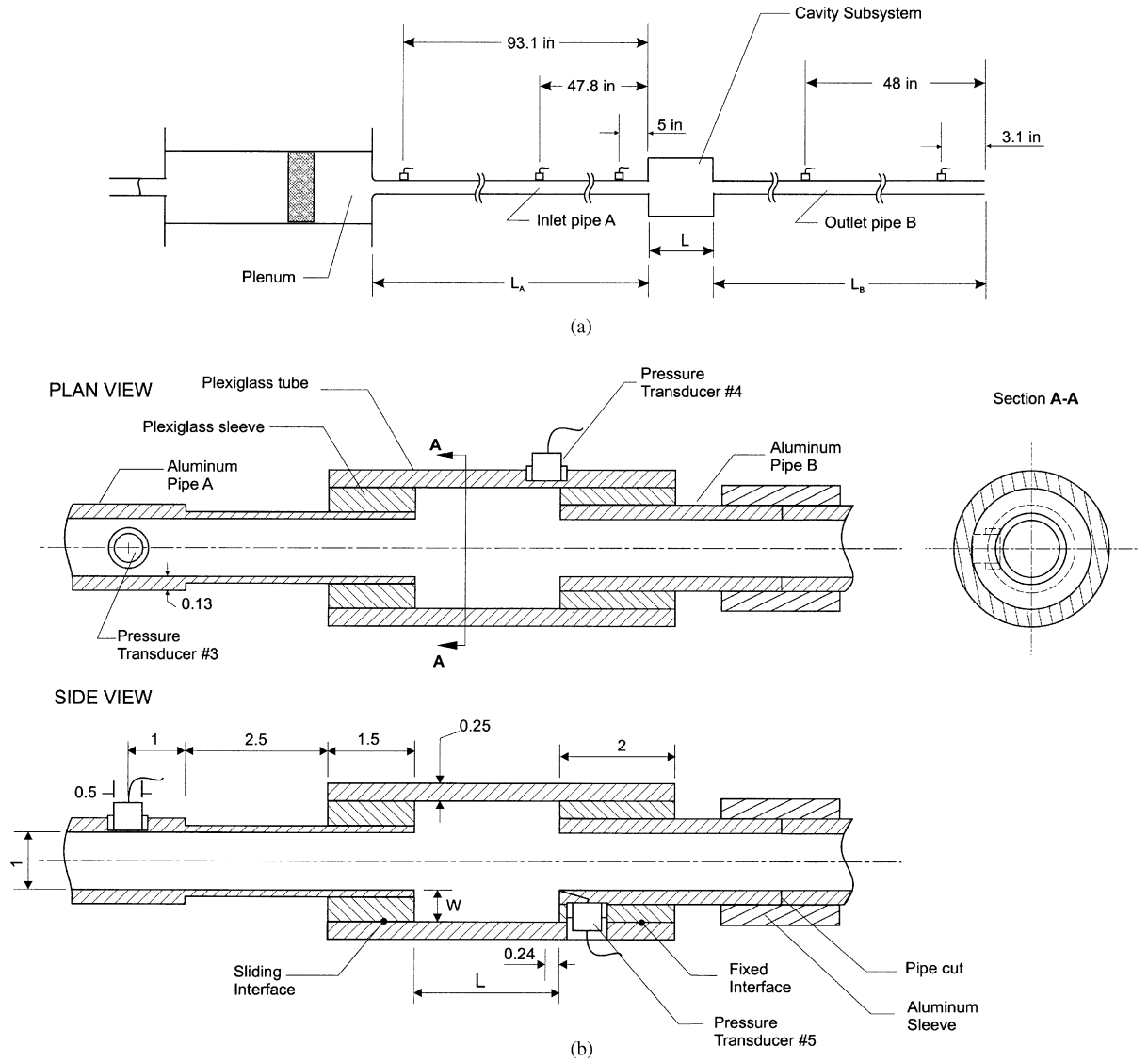

Fig. 1. (a) Simplified schematic of the pipeline–cavity system, and (b) details of cavity subsystem.

inlet of the cavity subsystem and a pipe of length L_B at the outlet. These pipes had an internal diameter (ID) of 1 in (25.4 mm) and a wall of thickness 0.2 in (5.1 mm). The long-pipe system involved pipes of length $L_A = L_B = 8$ ft (2.4 m). The short-pipe system corresponded to $L_A = L_B = 12$ in (30.48 cm). The locations of multiple pressure transducers in the long- and short-pipe systems are addressed in detail by Rockwell et al. [8]. Unless otherwise indicated, all pressure signals in the present investigation correspond to the most representative location in the pipeline resonator. This location was at a distance of 5 in (127 mm) upstream of the inlet pipe exit, as illustrated in Fig. 1a.

2.3. Cavity subsystem

Rockwell et al. [8] provide details of the cavity subsystem. A brief summary is provided here. The schematic of the cavity subsystem is provided in Fig. 1(b). The inlet (upstream) pipe A was fixed to the pipe supports and remained stationary throughout all experiments. On the other hand, the outlet (downstream) pipe B was mounted on a traverse mechanism, in order to accommodate variations in cavity length L. The cavity is formed by a plexiglas tube, which fits over two plexiglas sleeves. The left sleeve is fixed to the aluminum pipe A. The interface between this sleeve in the plexiglas tube is, however, a sliding interface, in order to allow variations of cavity length L. Regarding the right-hand plexiglas sleeve, it is fixed to both the aluminum pipe B and the plexiglas tube. The advantage of this design is that the pressure transducers #4 and #5, indicated in Fig. 1(b), remain at fixed locations with respect to the impingement corner of the cavity, while the cavity length L is varied. Both pipes A and B have an internal diameter of 1 in (25.4 mm).

Of primary interest in the present investigation is variation of the dimensionless depth of the cavity, i.e., $W/D = 1.25$, 0.5, 0.25 and 0.125, in which D is the pipe diameter. In order to accomplish this variation of W/D, it was necessary to machine four different sets of plexiglas sleeves at the ends of pipes A and B, as well as corresponding plexiglas tubes surrounding the sleeves.

Precise and repeatable variations of the cavity length L are required for a given value of cavity depth W. This was achieved by employing a traverse mechanism, which translated the entire pipe B and the plexiglas tube attached to it. This traverse mechanism was equipped with a Linear Variable Differential Transducer system, which allowed adjustment of the cavity length L on the basis of an amplified voltage display.

2.4. Pressure measurements

Pressure measurements inside the cavity, and along the inlet and outlet pipe sections were accomplished using a total of seven PCB transducers (Model No. U103A02) with a sensitivity of 1727 mv/psi. A 12-bit National Instruments board (Model PCI-MI0-16E-4) was utilized to digitize the conditioned pressure signals. The signals were processed on a Pentium II 350 MHz computer using LabView software.

During acquisition of the final experimental data, the sampling rate was set to 4096 samples/s, which resulted in a Nyquist frequency of 2048 Hz. To prevent aliasing effects, a low-pass filter was applied to all pressure signals. Each of the spectra represented herein is the result of averaging a total of 40 data sets, each containing 8192 data samples. The terminology spectra refer to plots of pressure amplitude versus frequency.

For a detailed description of pressure signal acquisition and processing, the reader is referred to Rockwell et al. [8].

2.5. Velocity measurements

The primary focus of the present investigation is measurement of unsteady pressure. It was, however, necessary to determine the averaged inflow velocity, in order to provide suitable

normalization of pressure amplitudes and to ensure that its magnitude was sufficient to trigger the onset of flow tones as cavity length L was varied.

The method used to determine the time-averaged centerline velocity $\bar{u}_m \equiv U$ involved calibration of the pressure difference between the interior of the inlet plenum and the exit of the nozzle located in the orifice plate, which was attached to the downstream end of the plenum. This pressure difference was plotted against the centerline velocity at the exit of the downstream pipe, which was determined using hot wire anemometry, and verified using a pitot probe in conjunction with a high-sensitivity pressure transducer at the exit of the pipe. This approach is described in detail in Rockwell et al. [8].

For the experiments described herein, a constant value of centerline velocity U was employed while the length of the cavity was varied. This value of velocity was either $U = 118$ or 130 ft/s. It ensured that tones would be excited over a range of cavity length L and depth W, as determined from extensive preliminary experiments, which are summarized by Rockwell et al. [8].

3. Inflow conditions

The present investigation addresses the generation of flow tones when the inflow is fully turbulent. Distributions of mean and fluctuating velocity at the exit of the inlet pipe, and associated definitions, are given by Rockwell et al. [8].

Specification of the inflow is important not only to ensure that it is fully turbulent, but also to properly scale the frequencies of the shear layer oscillation associated with generation of flow tones. The most common form of the dimensionless frequency of oscillation is fL/U or fD/U; L is the cavity length, U is the characteristic velocity, and D is the inlet pipe diameter. This type of scaling does not account for variations of the inflow boundary layer thickness that exist in different flow systems. The momentum thickness θ_0 is an appropriate characteristic thickness for separated shear flows. It is defined at the end of the inlet pipe, i.e., immediately prior to separation, as

$$\theta_0 = \int_0^\infty (\bar{u}/\bar{u}_m)(1 - \bar{u}/\bar{u}_m)\,\mathrm{d}y \tag{1}$$

in which $\bar{u}$ is the local time-averaged streamwise velocity and $\bar{u}_m$ is its value at the pipe centerline, i.e., U. The value of θ_0 is expected to be the appropriate scaling parameter in the initial region of disturbance growth, where a thin shear layer instability gives rise to shear layer or Kelvin–Helmholtz vortices.

The momentum thickness θ_0 was determined for two extremes of pipe length: (a) a long pipe, having a length-to-diameter ratio of 96, which yields a fully developed turbulent flow at the pipe exit; and (b) a relatively short pipe having a length-to-diameter ratio of 12, which has a turbulent boundary layer at its exit that is not fully developed. A boundary layer trip was positioned at the inlet of both of the long and short pipes. It ensured the rapid onset of turbulence. These two pipe lengths correspond to the two versions of the experimental system used in the present study. For the case of the long inlet pipe, the values of momentum thickness θ_0 normalized by the pipe radius R lie in the range $0.088 \leqslant \theta_0/R \leqslant 0.096$. For the case of the short inlet pipe, the dimensionless momentum thickness falls in the range $0.029 \leqslant \theta_0/R \leqslant 0.035$.

4. Overview of pressure fluctuations: effect of cavity length at constant values of cavity depth

The current study involves unsteady pressure fluctuations arising from flow past a shallow cavity. Nearly all previous investigations have considered the case where the cavity depth is much larger than the characteristic thickness of the inflow shear layer. When this is not the case, the cavity is shallow, and the mechanisms of onset and growth of the instabilities in the cavity shear layer may be influenced by the proximity of the floor of the cavity. Moreover, when the cavity length L is sufficiently small, large-scale vortices do not have the opportunity to develop in the cavity shear layer. This means that smaller-scale vortices formed in the separation region downstream from the leading corner of the cavity must effectively couple with the pipeline resonator if flow tones are to be generated. The present work is focused on the characterization of the unsteady pressures, and the possible occurrence of the flow tones, as a function of cavity length L and depth W.

4.1. Summary of ranges of parameters

The design of the cavity described in Section 2.2 allowed discrete values of cavity depth $W^* = W/D = 1.25, 0.5, 0.25, 0.125$. For each value of W^*, the inflow velocity $U \equiv \bar{u}_m$ was kept constant and the cavity length was varied over the range $0.25 \leqslant L/D \leqslant 2.5$. The incremental length was $\Delta L/D = 0.0625$. The largest value of L/D allows formation of large-scale vortices in the shear layer, and successively smaller values of L/D are presumably associated with smaller-scale modes of shear layer oscillations.

The value of inflow velocity $U \equiv \bar{u}_m$ was held at a sufficiently high value, such that the probability of triggering flow tones at each value of L was optimized. This value of U was 130 ft/s, as determined in the large-scale mode ($L/D = 2.5$) experiments of Rockwell et al. [8].

4.2. Methods of presentation of data

Pressure spectra are used to represent features of the unsteady fluctuations. For a given data set, a total of 37–40 spectra were acquired. As indicated in Section 2.4, the terminology spectra refer to plots of amplitude versus frequency. Each spectrum corresponded to a different value of cavity length L. A color coded, isometric view (shown here in shades of grey) was developed for comprehensive presentation of families of spectra. The top image of Fig. 2 is an example of this representation. The values of spectral amplitude are interpolated along the cavity length axis. The color coding of the amplitude values was designed such that most of the changes in color level are concentrated at the lower values of pressure amplitude. This approach emphasizes the onset of flow tones.

The bottom graph of Fig. 2 is a plan view of the isometric plot. This type of plan view is provided for each set of experimental data. It allows examination of pressure peaks on a plane of cavity length L versus frequency f, and gives a rapid indication of the extent of each region of highly coherent oscillation, or flow tone generation. The lines superposed on this plot pass through the peaks. In regions where the peaks are not immediately evident, a gradient detection method was employed as described by Rockwell et al. [8].

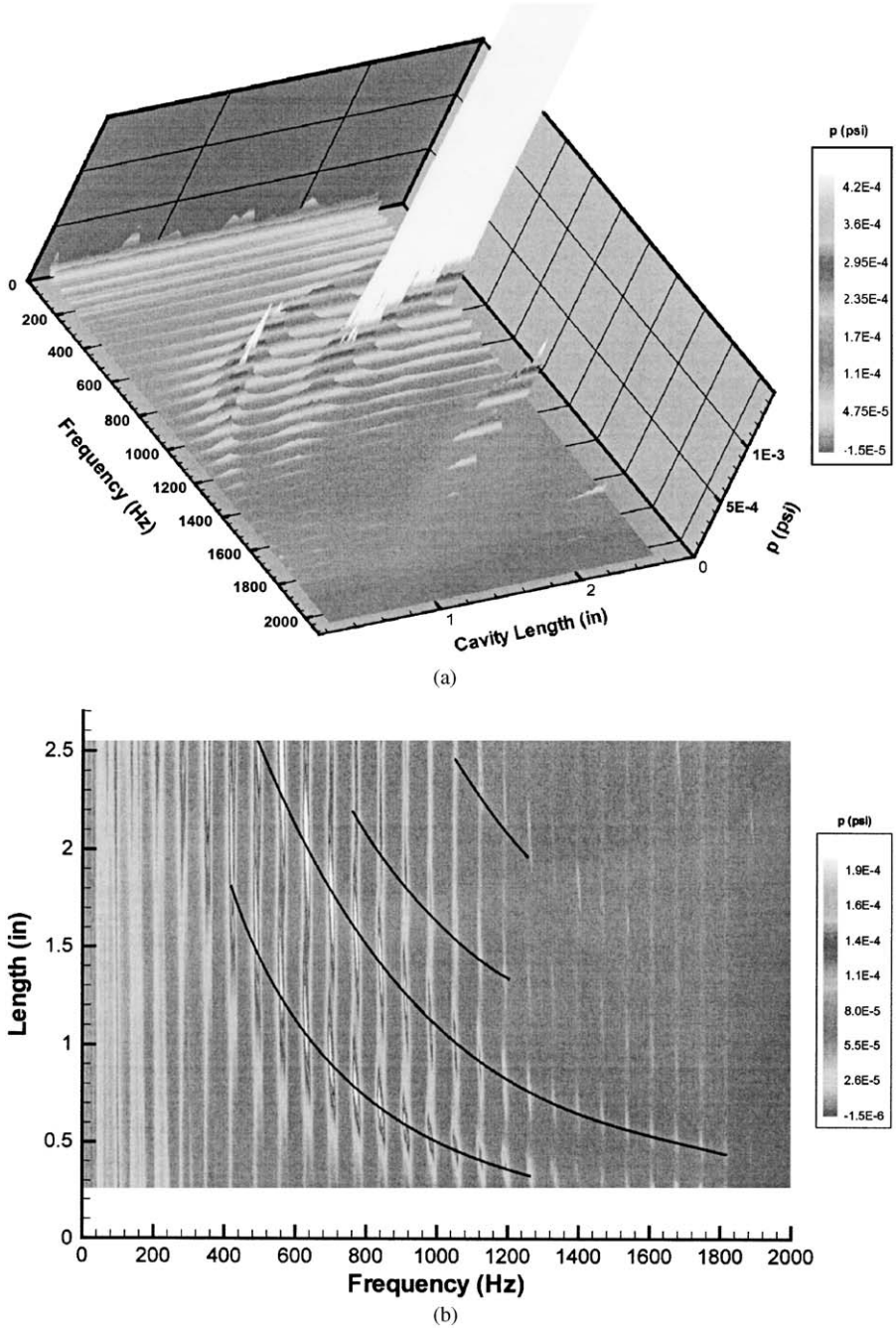

Fig. 2. (a) Isometric view, and (b) plan view of pressure amplitude as a function of frequency and cavity length. Lines shown on plan view represent fits through peak values of pressure amplitude. Long–long pipe; cavity $W = 1.25\,\text{in}$; velocity $U = 130\,\text{ft/s}$.

4.3. Pressure fluctuations for variations of cavity length

The primary thrust of the present effort is to characterize the self-sustained oscillations as a function of cavity length L at discrete values of cavity depth W. These oscillations must, however, be considered in the context of the momentum thickness θ_0 of the inflow boundary layer. As described in Section 3, use of a long pipe at the inlet of the cavity yields a dimensionless momentum thickness nearly three times as large as for the case of a short pipe. This approach allows examination of the effect of normalized cavity length L/θ_0 and depth W/θ_0, relative to the geometric normalizations L/D and W/D. In addition, use of long pipes at the inlet and outlet of the cavity yield closely spaced resonant acoustic modes, relative to the case of short pipes, where the modes are relatively widely spaced. In the following, the cases of long- and short-pipe–cavity systems are examined for variations of cavity length L for discrete values of cavity depth W.

4.3.1. Long inlet pipe–cavity system

Figs. 2–5 show the effect of variations of cavity length L for successively decreasing values of cavity depth W, while the inflow velocity U is maintained constant.

Fig. 2 represents the case of the deepest cavity $W/D = 1.25$. As shown in the three-dimensional plot of Fig. 2, two clearly defined Strouhal trends, i.e., families of peaks following constant fL/U, are clearly identifiable. The leftmost series of peaks shown in the upper image of Fig. 2 are detectable down to relatively small values of cavity length L; in fact, they are discernible for values of $L \gtrsim 0.5$ in. This indicates that the instability in the jet is detectable at small values of cavity length L. It is clear, from the three-dimensional representation of Fig. 2, that the dominant pressure amplitude occurs at the largest values of cavity length, generally for $L \gtrsim 2$ in. These large amplitudes are apparently due to sufficiently mature, large-scale vortices that develop along the mouth of the cavity, as discussed by Rockwell et al. [8].

The lower image of Fig. 2 represents a plan view of pressure amplitude on a plane of cavity length versus frequency. It is clear from the plan view of Fig. 2 that the lowest two lines of constant fL/U define the centers of regions of high-pressure amplitude, i.e., localized white regions. These white regions generally occur over a frequency range extending from approximately 550–800 Hz. This range of predominant pressure peaks holds for both of the bottom Strouhal lines of Fig. 2. In addition, Fig. 2 shows two additional Strouhal lines that occur at larger length L. They were determined with the aid of a gradient detection method, described by Rockwell et al. [8]. The case of a shallower cavity, corresponding to $W/D = 0.5$, is exhibited in Fig. 3. The three-dimensional image shows a generally similar form as for the deepest cavity of Fig. 2. That is, two Strouhal lines are suggested by the variations of peak pressure amplitudes with cavity length L. Moreover, the largest amplitudes again occur at relatively long cavity lengths, of the order of $L \gtrsim 2$ in. The lower image of Fig. 3 gives a plan view of pressure amplitude (linear scale) on the cavity length versus frequency plane, clearly shows that the predominant pressure peaks occur approximately in the frequency range extending from 500 to 900 Hz. Fig. 4 corresponds to a further decrease in cavity depth to $W/D = 0.25$. Detectable peaks occur, as indicated in the three-dimensional representation of Fig. 4. These peaks are, however, of very low magnitude. Moreover, these small amplitude peaks suggest three Strouhal variations, corresponding to $fL/U =$ constant. In fact, lines corresponding to these variations are shown in the plan view of the bottom image of Fig. 4. Comparison of the top and bottom images of Fig. 4

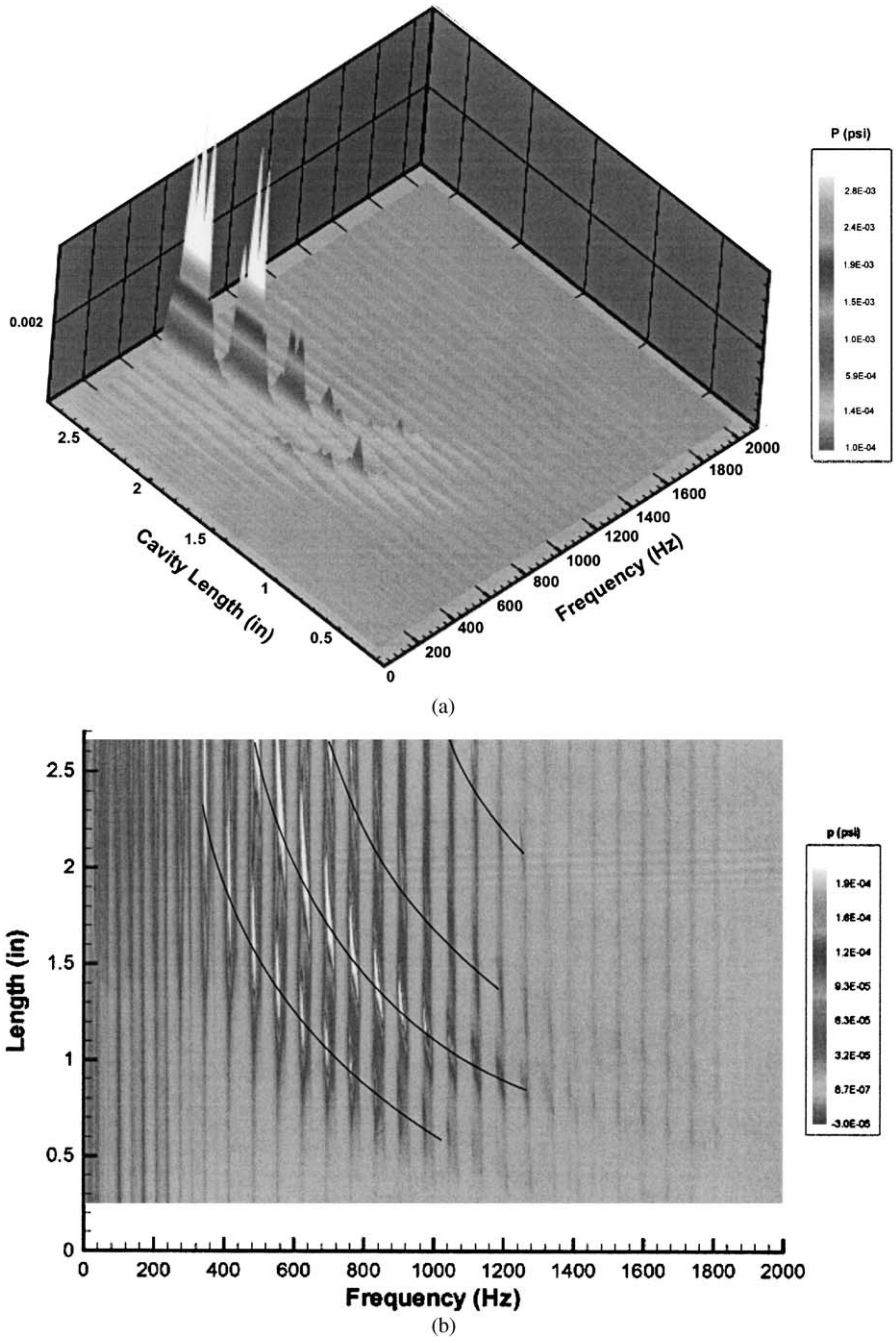

Fig. 3. (a) Isometric view, and (b) plan view of pressure amplitude as a function of frequency and cavity length. Lines shown on plan view represent fits through peak values of pressure amplitude. Long–long pipe; cavity $W = 0.5\,\text{in}$; velocity $U = 130\,\text{ft/s}$.

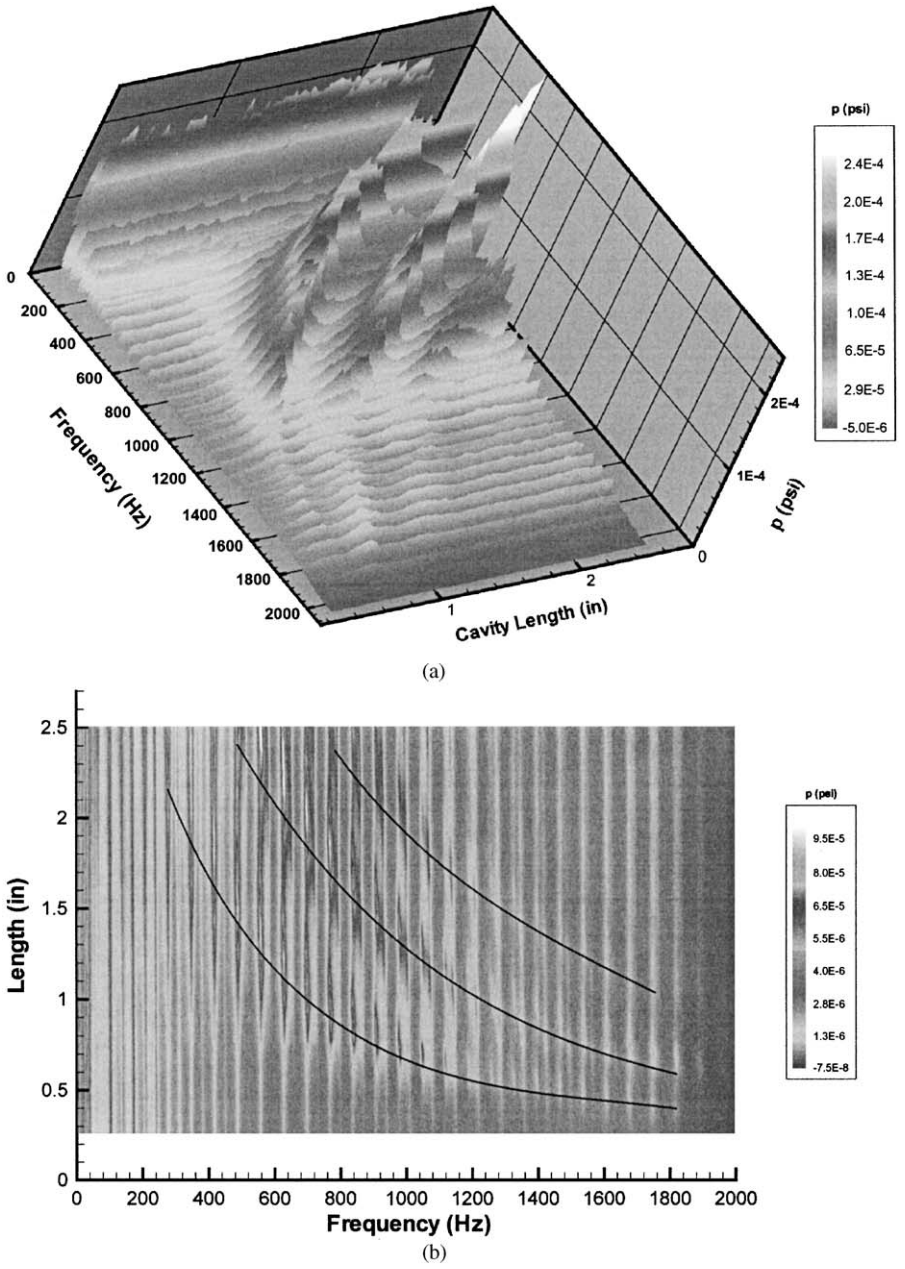

Fig. 4. (a) Isometric view, and (b) plan view of pressure amplitude as a function of frequency and cavity length. Lines shown on plan view represent fits through peak values of pressure amplitude. Long–long pipe; cavity $W = 0.25$ in; velocity $U = 130$ ft/s.

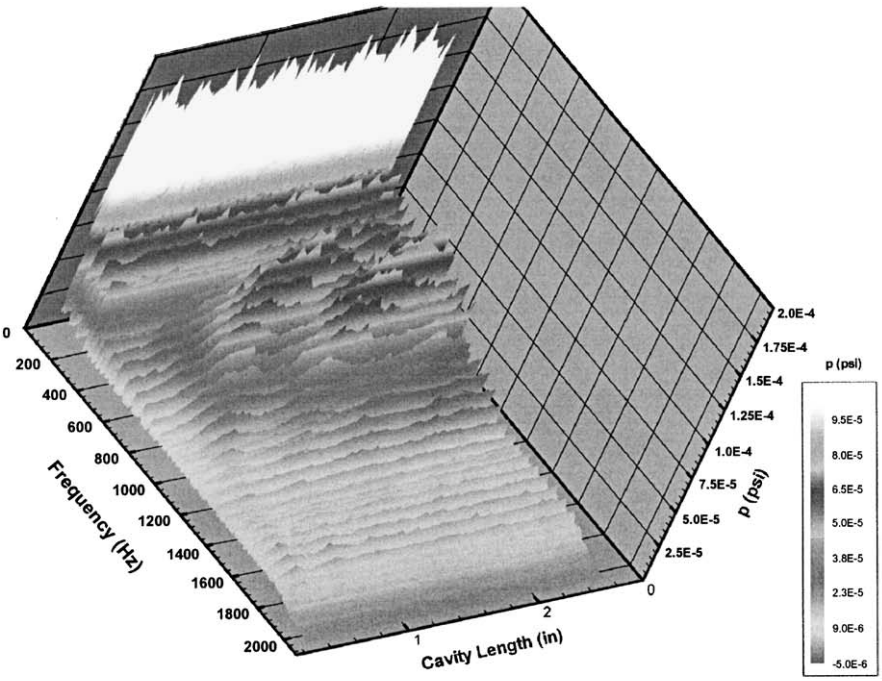

(a)

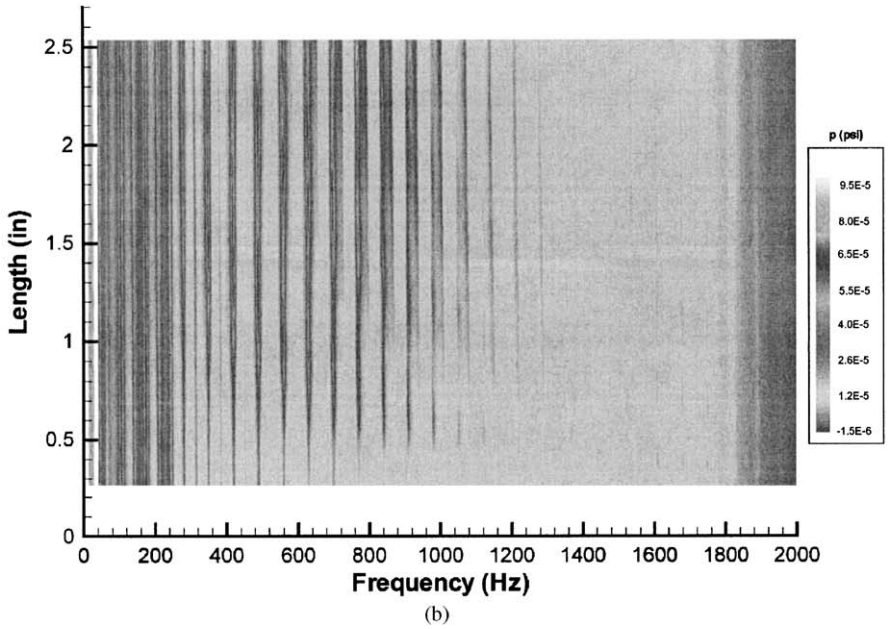

(b)

Fig. 5. (a) Isometric view, and (b) plan view of pressure amplitude as a function of frequency and cavity length. Long–long pipe; cavity $W = 0.125$ in, velocity $U = 130$ ft/s.

shows that the major peaks occur at frequencies ranging from 500 to 800 Hz. Moreover, the largest peaks occur at the longest values of cavity length $L \gtrsim 2$ in.

The smallest value of cavity depth $W/D = 0.125$, represented by Fig. 5, still suggests a Strouhal-like variation at sufficiently large values of cavity length L and low frequency f. In these cases, the peak values of pressure amplitude are extremely small, and the pattern of peaks shown in Fig. 5 is sufficiently ill-defined that it is not possible to construct Strouhal lines in the plan view of the bottom image of Fig. 5.

An overview of the three-dimensional representations of the pressure amplitude on the plane of cavity length versus frequency is exhibited in Fig. 6. For purposes of brevity, the case $W/D = 0.5$, which is generally similar to $W/D = 1.25$, is not included. This comparison directly shows the transformation from large-amplitude, sharply defined peaks at longer values of cavity length L to low-amplitude discernable peaks at small L, provided the cavity depth W is sufficiently large, i.e., $W/D = 1.25$. As W becomes smaller, i.e., $W/D = 0.25$, peaks at larger L are not as sharp as those

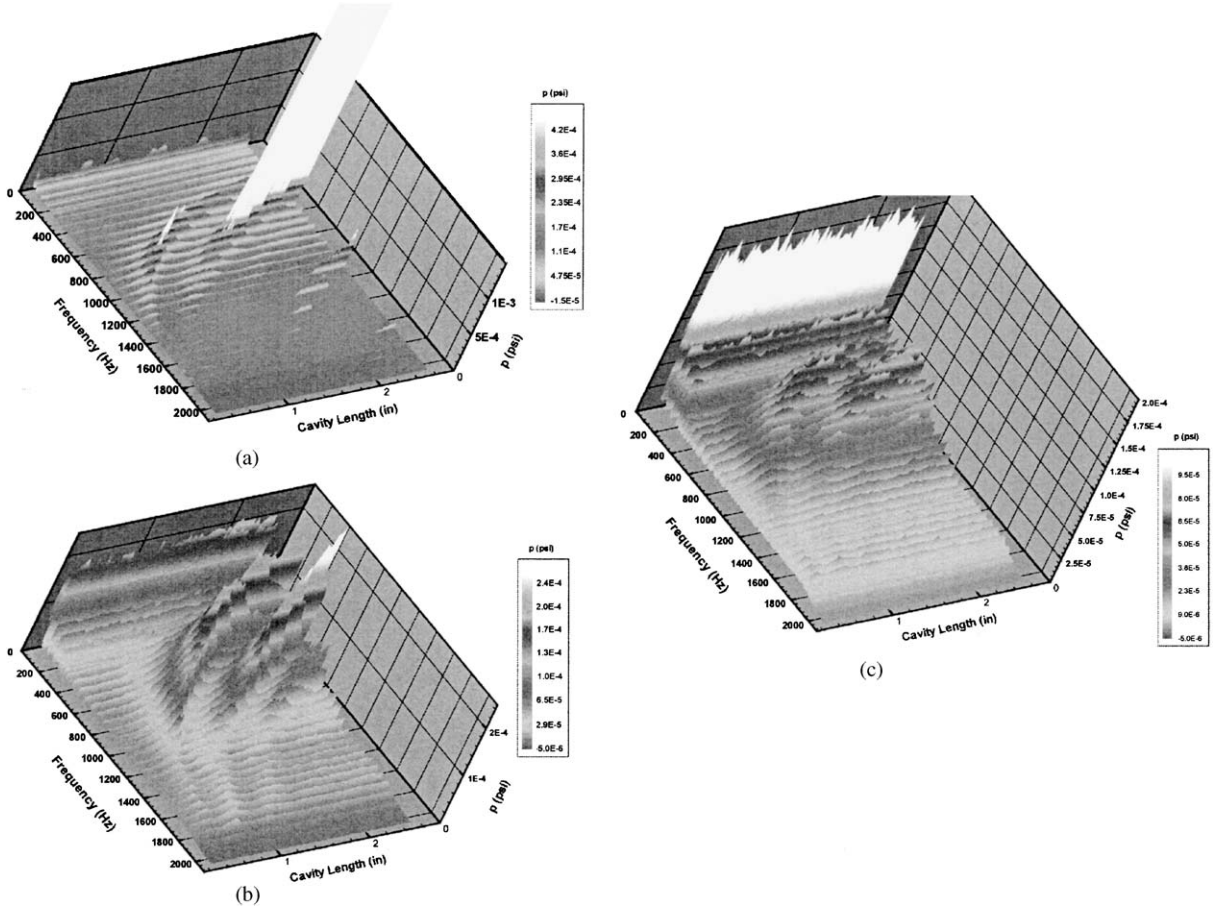

Fig. 6. Overview effect of cavity depth on three-dimensional representation of pressure amplitude as a function of velocity and cavity length. In all cases, the inflow velocity U is maintained constant. The cavity length varies from 0.25 to 2.5 in and cavity depth has values of (a) $W = 1.25$ in, (b) 0.25 in, and (c) 0.125 in.

for $W/D = 1.25$. Nevertheless, the peak amplitudes are substantially attenuated with decreasing values of L. Finally, for the shallowest cavity, $W/D = 0.125$, the peaks are even less-sharply defined but, remarkably enough, a trend of the two predominant modes with decreasing L is discernible, and it is in general accord with the trend for the cavities that have larger values of $W/D = 0.25$ and 1.25.

The overall features of the pressure fluctuations described in this section provide a basis for scaling the observed frequencies and amplitudes of spectral peaks. Appropriate dimensionless representations of the frequencies of pressure peaks will be addressed in Section 5. Maximum dimensionless amplitudes of the peaks are addressed in Section 6.

4.3.2. Short inlet pipe–cavity system

Figs. 7–10 show the pressure response characteristics for the case of the short inlet pipe. In essence, as described in the previous section, this inflow configuration produces a boundary layer having a momentum thickness θ_0 that is approximately one-third of that corresponding to the fully developed turbulent flow at the end of the long inlet pipe.

The top image of Fig. 7 shows a three-dimensional view of the pressure amplitude response for the deepest cavity $W/D = 1.25$. As for the case of the long inflow pipe, addressed in Fig. 2, large amplitude peaks are evident for the longest cavity lengths $L \gtrsim 2$ in. Moreover, the approximate value of frequency, $f = 600$ Hz, is roughly the same value as that of Fig. 2 for the case of the large amplitude peak from the long inlet pipe. In addition, sharply defined peaks are now evident at relatively small values of cavity length L and at higher values of frequency f. In the limit, a clearly defined peak is evident for $L \simeq 0.5$ in. and, for larger values of L as well. The plan view of pressure amplitude on a plane of cavity length versus frequency, corresponding to the bottom image of Fig. 7, shows that these higher-frequency peaks are centered on resonant frequencies of the order of 1100–1200 and 1600–1700 Hz. Moreover, it is possible to define lines of constant Strouhal frequency fL/U, as indicated in the bottom image of Fig. 7. Fig. 7 suggests that flow tones may be generated at relatively small values of cavity length L. The issue then arises as to what degree the shallowness of the cavity, represented by cavity depth W, allows these oscillations to be sustained.

The case of a shallower cavity, corresponding to $W/D = 0.5$, is indicated in Fig. 8. It shows a three-dimensional representation, which can be compared directly with the case of the deepest cavity shown in Fig. 7. It is evident that, with some exceptions, the overall response characteristics are generally similar. The occurrence of the largest amplitude peaks for $L \gtrsim 2$ in, centered at a frequency of approximately $f = 550$ Hz, is still present. Moreover, at the other extreme, for small values of cavity length, $L \simeq 0.5$ in, a pronounced peak is still evident. As indicated in the bottom image of Fig. 8, it is possible to construct constant Strouhal lines, i.e., constant fL/U through the peaks, as indicated.

The case of a still shallower cavity, represented by $W/D = 0.25$, is shown in Fig. 9. This three-dimensional plot has major features that are generally similar to those described in Fig. 8. That is, the occurrence of pronounced flow tones at extreme values of cavity length L, and the frequencies at which they arise, is in overall agreement.

The limiting case of the shallowest cavity, corresponding to $W/D = 0.125$, is shown in Fig. 10. It is clear from the top image that sharply defined peaks do not occur, unlike those shown in the three-dimensional plots of Figs. 7–9. It is interesting to note, however, that discernible peaks do occur; they have the largest relative magnitudes at longer values of cavity length L, and at lower

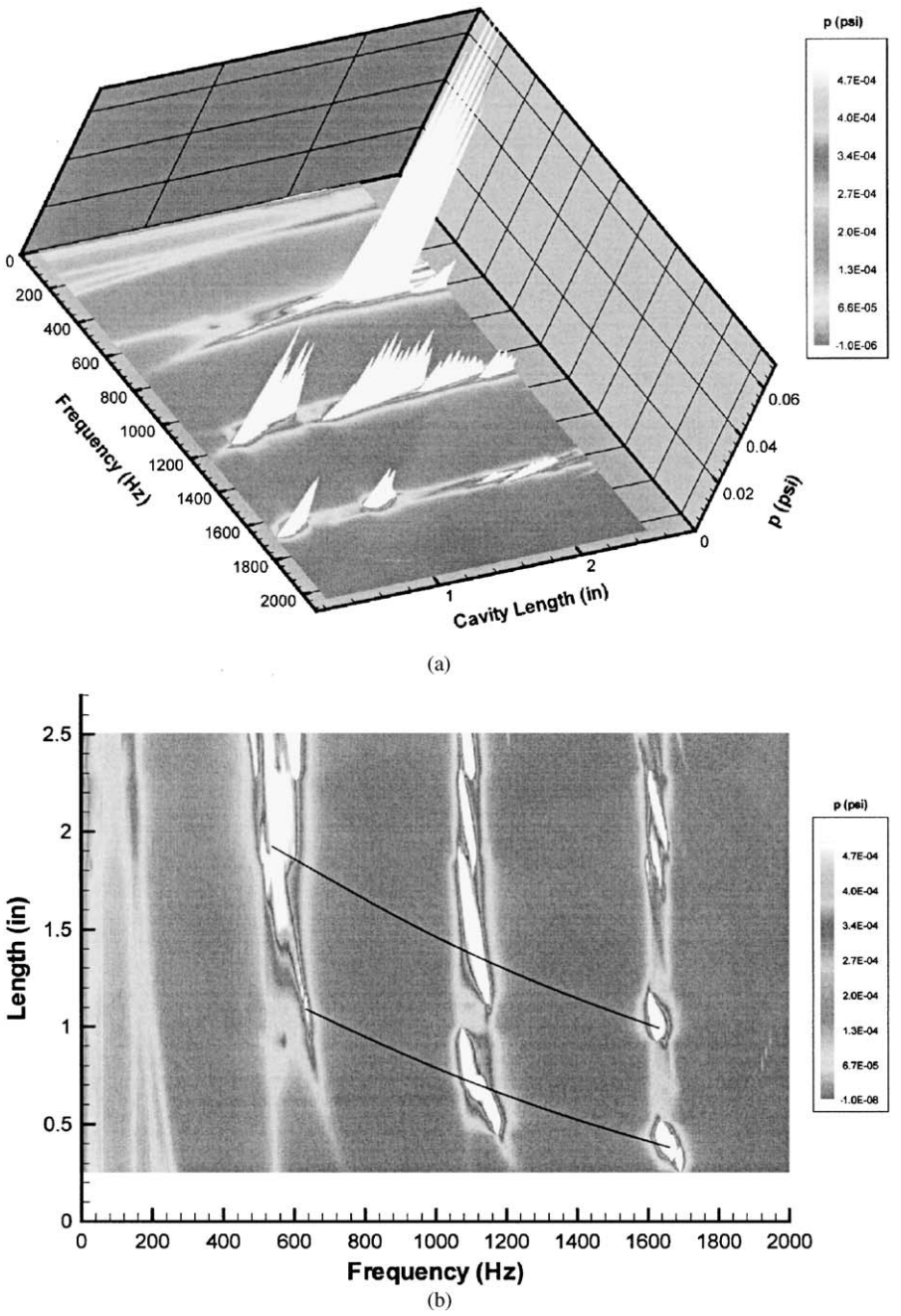

Fig. 7. (a) Isometric view, and (b) plan view of pressure amplitude as a function of frequency and cavity length. Lines shown on plan view represent fits through peak values of pressure amplitude. Short–short pipe; cavity $W = 1.25$ in; velocity $U = 130$ ft/s.

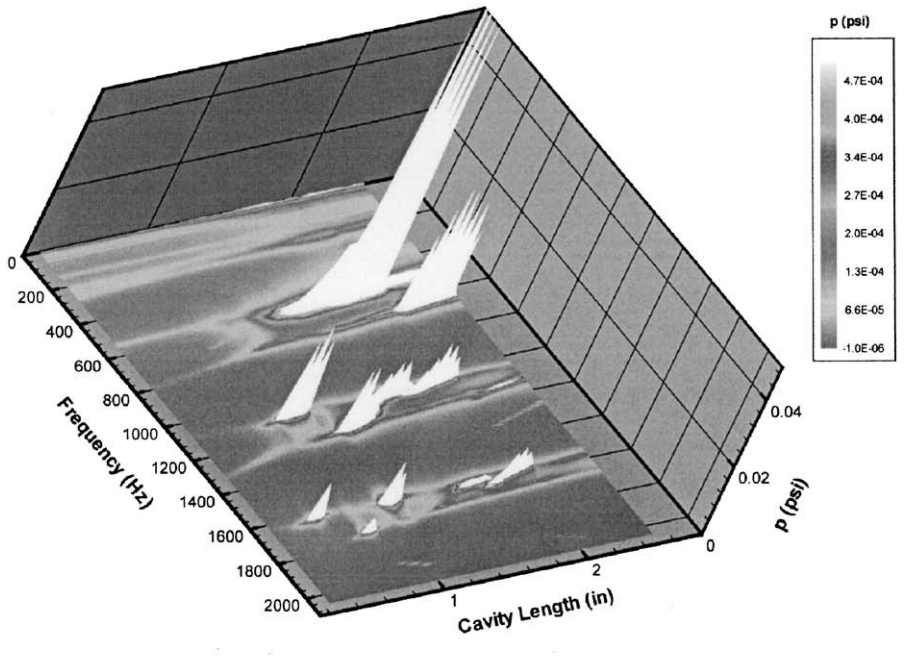

(a)

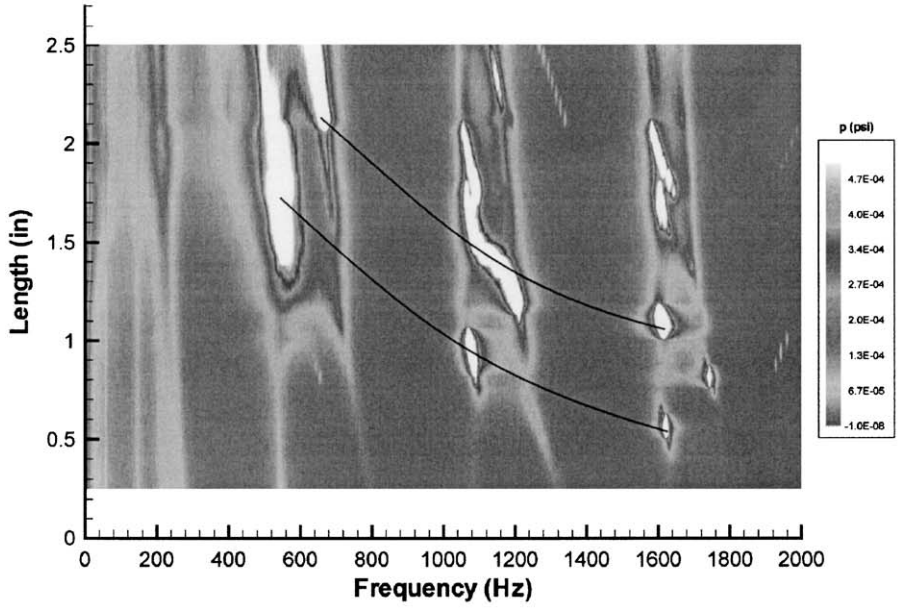

(b)

Fig. 8. (a) Isometric view, and (b) plan view of pressure amplitude as a function of frequency and cavity length. Lines shown on plan view represent fits through peak values of pressure amplitude. Short–short pipe; cavity $W = 0.5$ in; velocity $U = 130$ ft/s.

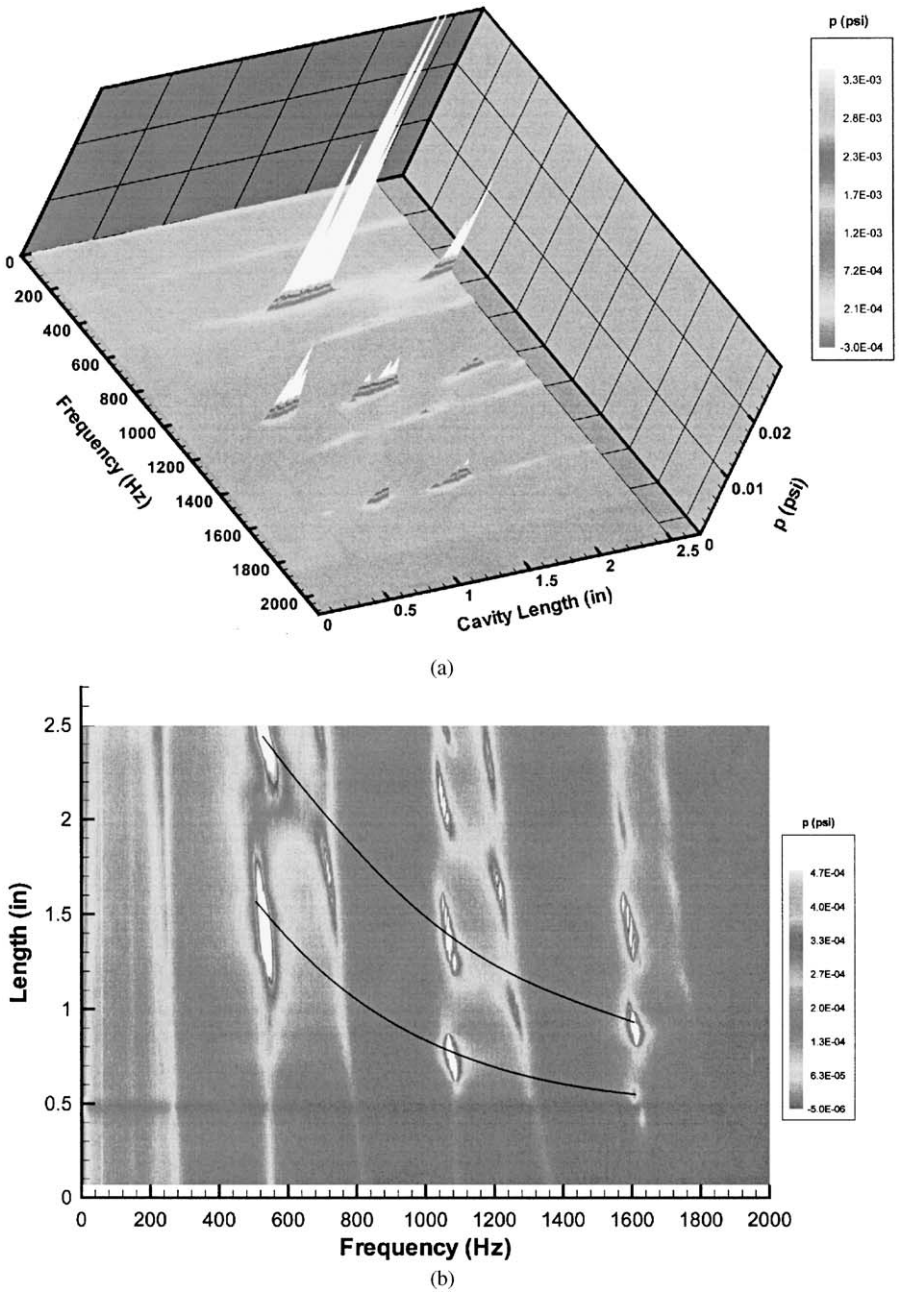

Fig. 9. (a) Isometric view, and (b) plan view of pressure amplitude as a function of frequency and velocity. Lines shown on plan view represent fits through peak values of pressure amplitude. Short–short pipe; cavity $W = 0.25$ in; velocity $U = 118$ ft/s.

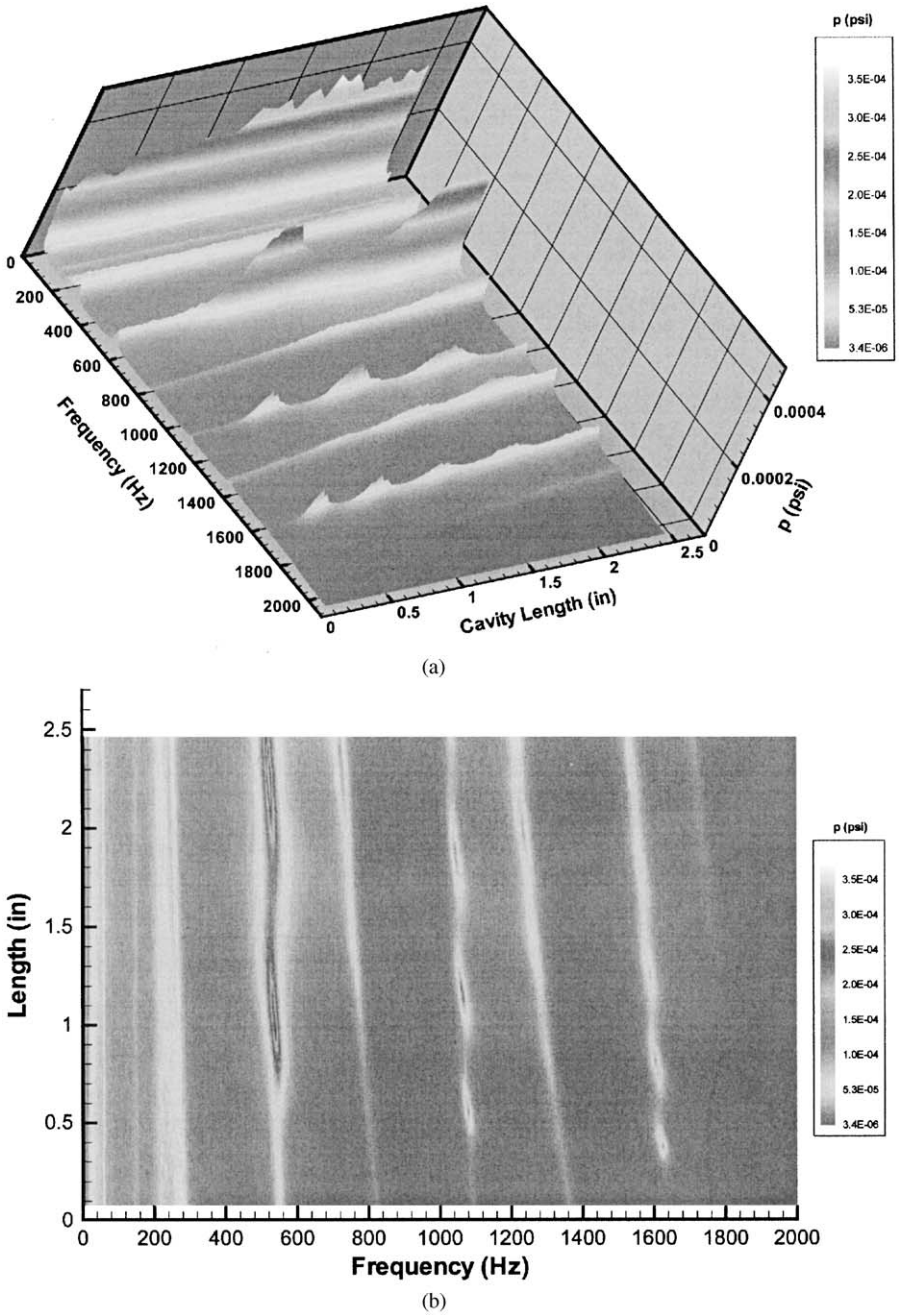

Fig. 10. (a) Isometric view, and (b) plan view of pressure amplitude as a function of frequency and cavity length. Short–short pipe; cavity $W = 0.125$ in; velocity $U = 118$ ft/s.

frequencies of the order of 550 Hz. In other words, even though flow tones are not generated at the shallowest cavity depth, the tendency to generate relatively low-level quasi-coherent oscillations is still present. In comparison with the plots of Figs. 7–9, however, the absolute pressure amplitudes in Fig. 10 are very low.

The dimensionless frequencies and amplitudes of the pressure peaks described in the foregoing are characterized in Sections 5 and 6.

The acoustic properties of the pipeline system can be characterized by employing the quality (Q) factor of the resonant acoustic modes. The Q-factor is determined by the following relationship: $Q = f_0/(f_2 - f_1)$, where f_0 is the resonant frequency, and f_1 and f_2 are the frequencies below and above the resonant frequency at which the average power is one-half of the average power at resonance. In presence of flow, but in absence of any coupling between flow unsteadiness and a resonator, the quality factor Q of the pressure response spectrum cannot have a quality factor exceeding Q of the resonator. In principle, this criterion provides a basis for determining the occurrence of the initial state of lock-on, provided uncertainties in deviations of evaluated Q-factors are accounted for. The nominal, upper limit of the Q-factors for the data presented in this section approximately corresponds to the theoretically determined value in absence of mean flow. Values of Q-factor can extend substantially below this limit due to the effects of mean flow. On the basis of the acquired data, values of Q-factor substantially in excess of $Q = 180$ are taken to represent occurrence of a locked-on state. In fact, considering the entire range of data displayed in Figs. 2–10, the smallest value of Q-factor of the well-defined peak amplitudes is $Q = 350$, and the maximum value is $Q = 2000$.

5. Correlation and scaling of oscillation frequencies

5.1. Correlations of frequencies of oscillation with existing models based on cavity length

The frequency f of the pressure fluctuation can be cast in dimensionless form by use of the cavity length L and the inflow velocity U, i.e., fL/U. This representation is related to the overall features of the instability wave or vortex system along the mouth of the cavity. It can provide guidance on the variation of not only the predominant mode of oscillation, but also multiple, coexisting modes, as a function of cavity length L.

5.1.1. Summary of models

Traditional semi-empirical models, as well as recent theoretically based models, for the dimensionless frequency of oscillation have the general form

$$fL/U = (U_c/U)(n + a) \tag{2}$$

in which U is taken to be the free-stream velocity, U_c is the convective speed of a vortex or instability wave through the shear layer, n is the stage of oscillation and a is an end correction. This type of relationship has been traditionally employed for open cavity and jet-edge configurations. Recently, Rockwell et al. [8] implemented the models of this type in their study of the onset of flow tone lock-on for the case of axisymmetric cavity mounted in a pipe. The

historical development and application of this type of model, which includes the theoretical approach of Howe [5,6], are addressed by Rockwell et al. [8].

It should be noted that the above-mentioned relationships are based on the linear stability theory, and therefore can be directly applied only to the cases where the acoustic velocity values are small relative to the values of the free-stream velocity. In the current study, these correlations are employed for the purposes of comparison and as a means of illustration of the coexistence of the multiple modes of oscillation. The following models are used in the present investigation: $fL/U = 0.6(n - 1/4)$ from Elder [13] and Pollack [17]; (b) $fL/U = 0.6(n + 1/6)$ from Howe [5,6]; and (c) $fL/U = 0.6n$ from Rockwell and Schachenmann [26].

Rockwell et al. [8] considered two approaches to frequency normalization for the above-mentioned models. These experiments involved internal flow in a pipe–cavity system; the velocity was varied at a constant value of cavity length. One approach involved normalization with respect to the averaged centerline velocity U of the pipe. The other method involved normalization with respect to the averaged velocity $0.86U$. The current study employs $0.86U$ as the velocity for normalization. The next section compares the above-mentioned correlations with the data of Section 4.3.

5.1.2. Correlations for variations of cavity length

The plots of Figs. 11–13 show correlation for the case of the long inlet pipe. Fig. 11 represents the deepest cavity $W/D = 1.25$, which was described in Fig. 2. The top plot of Fig. 11 shows that as many as four simultaneous modes are detectable. These lines correspond to a simple fit through the experimental data. This fit has the form $fL/U = K$, where K is a constant that provides the best approximation to the data variation in each mode. The shaded region identifies the three data points corresponding to the pressure peaks having maximum amplitude, i.e., the peaks shown in Fig. 2. In other words, when cavity length L is increased to a sufficiently large value, large amplitude peaks of the pressure occur.

The bottom plot of Fig. 11 shows the comparison between the data and the relationships defined in Section 5.1. No single relationship provides a universal fit for all modes of the data. In fact, it appears that the mode associated with the dominant pressure amplitudes, designated by the hollow circular symbols, undergoes a transformation from what appears to be an $n = 1$ mode to an $n = 2$ mode as cavity length L is increased.

The case of a shallower cavity $W/D = 0.5$ is shown in Fig. 12. Similar observations hold as for Fig. 11, with some distinctions. Again, no single equation provides a universal correlation for all modes. The mode associated with the dominant amplitudes does, however, tend to follow the $n = 2$ curve, corresponding to the $(n-1/4)$ equation.

A still further decrease in the depth of the cavity to a value $W/D = 0.25$ is represented in Fig. 13. In this case, only three identifiable modes $n = 1$, 2, and 3 are detectable. The frequencies that correspond to the dominant amplitude peaks show a generally similar range of values as for the deeper cavity, i.e., Fig. 12.

Fig. 14 represents case of the short inlet pipe, as opposed to the long inlet pipe. The cavity depth has an intermediate value of $W/D = 0.5$. The observations described in the following are generally valid for other cavity depths as well.

Since the resonant acoustic modes of the pipe–cavity system are relatively widely spaced, only three resonant modes, i.e., three sets of data points, are evident in Fig. 14 as the cavity length L is

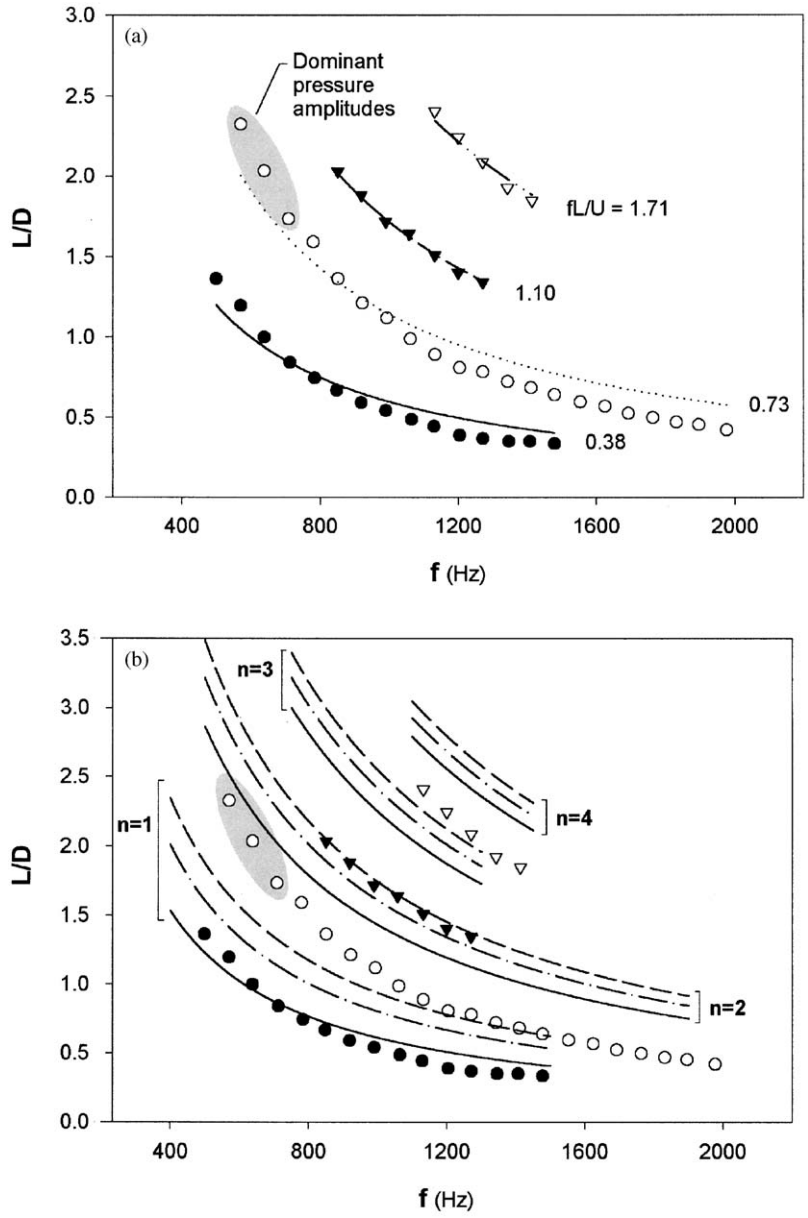

Fig. 11. Plots of values of frequency corresponding to identifiable peaks in Fig. 2. Top plot (a) shows best fit through values of frequency for each mode fL/U = constant. Bottom plot (b) shows curves corresponding to correlations for fL/U. (—) $fL/(0.86U) = 0.61(n-1/4)$; (- - -) $fL/(0.86U) = 0.61(n+1/6)$; (– · – · –) $fL/(0.86U) = 0.61n$. The shaded regions indicate dominant pressure amplitudes corresponding to largest peaks in the plot of Fig. 2.

varied. As for the cases of the long inlet pipe, simple fits to the data of the form $fL/U = K$ are provided (top plot) as well as comparison of the data with the models described in Section 5.1 (bottom plot).

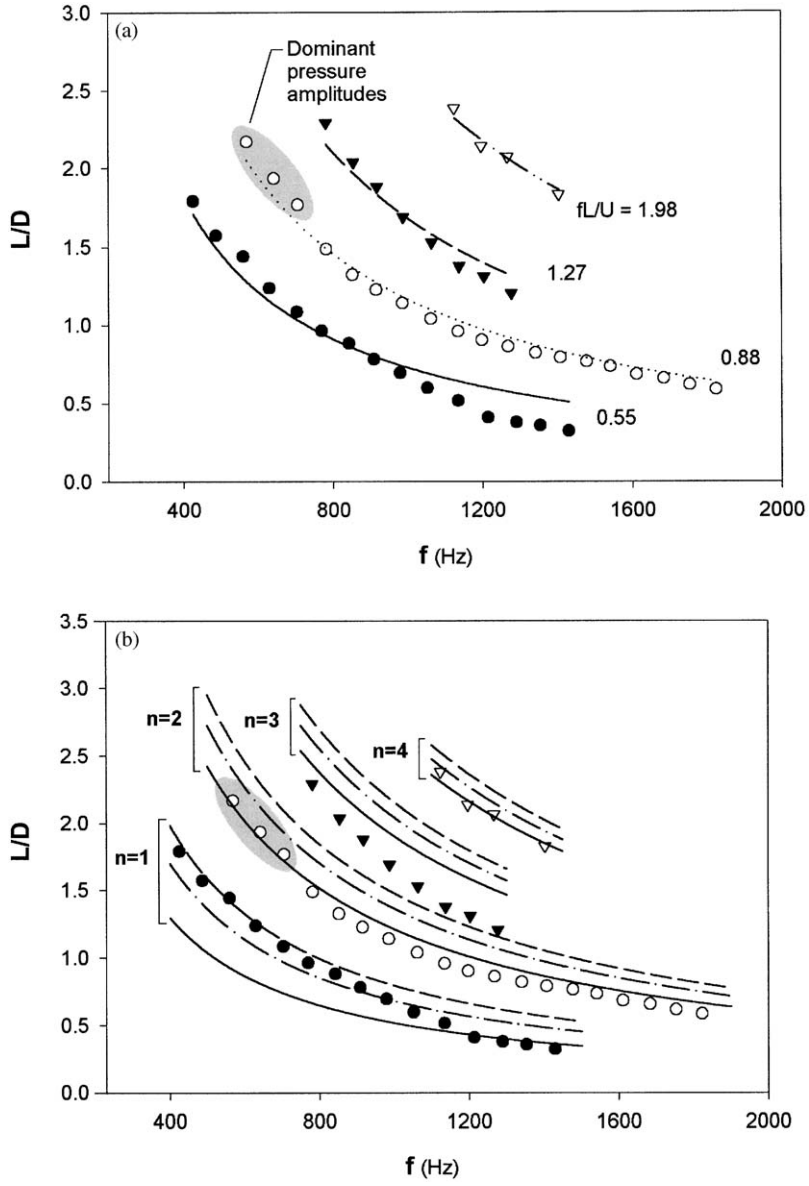

Fig. 12. Plots of values of frequency corresponding to identifiable peaks in Fig. 3. Top plot (a) shows best fit through values of frequency for each mode $fL/U=$constant. Bottom plot (b) shows curves corresponding to correlations for fL/U. (—) $fL/(0.86U)=0.61(n-1/4)$; (- - -) $fL/(0.86U)=0.61(n+1/6)$; (–·–·–) $fL/(0.86U)=0.61n$. The shaded regions indicate dominant pressure amplitudes corresponding to largest peaks in the plot of Fig. 3.

In addition to the dominant amplitudes of the pressure peaks, the so-called onset of pressure peaks is also designated. This terminology is used to indicate sharply defined peaks, albeit of smaller amplitude, that arise at smaller values of L.

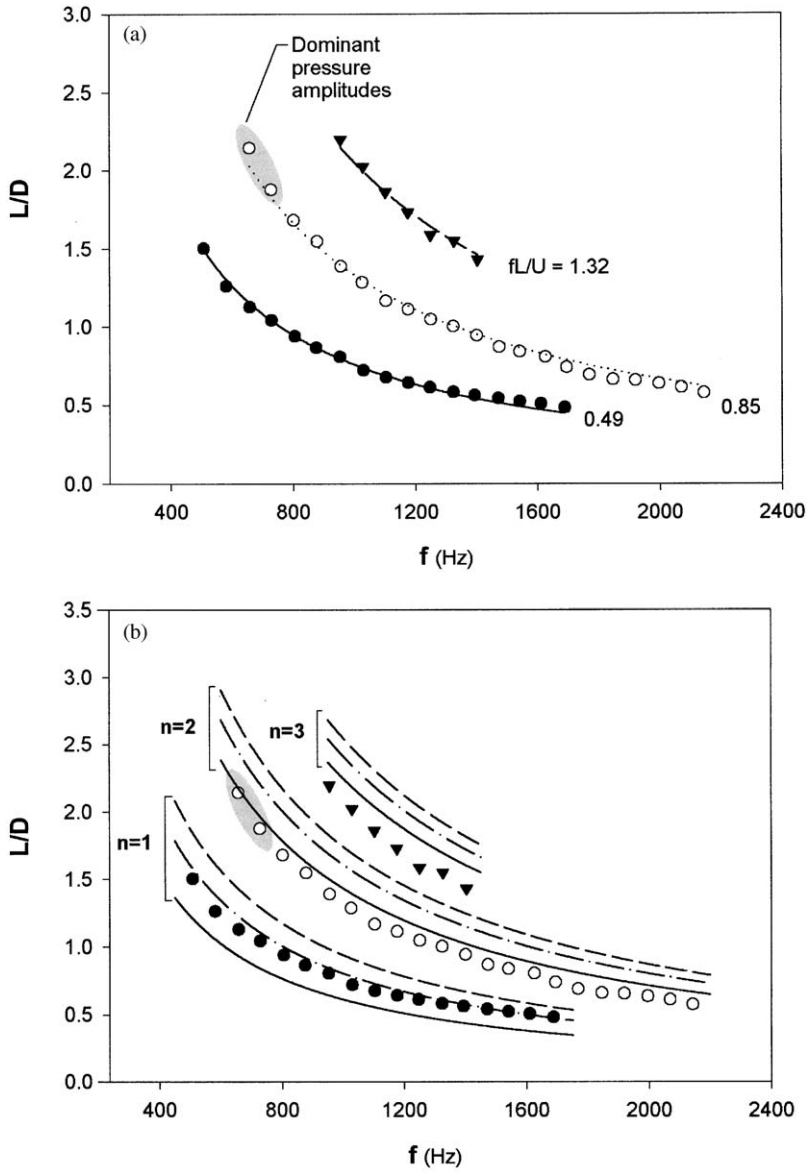

Fig. 13. Plots of values of frequency corresponding to identifiable peaks in Fig. 4. Top plot (a) shows best fit through values of frequency for each mode fL/U = constant. Bottom plot (b) shows curves corresponding to correlations for fL/U. (—) $fL/(0.86U) = 0.61(n-1/4)$; (- - -) $fL/(0.86U) = 0.61(n+1/6)$; (–·–·–) $fL/(0.86U) = 0.61n$. The shaded regions indicate dominant pressure amplitudes corresponding to largest peaks in the plot of Fig. 4.

6. Assessment of multiple modes of cavity oscillation

The data described above show existence of two or more modes at a given value of cavity length L. Three different scaling approaches are employed to construct the representations of Figs. 15–17.

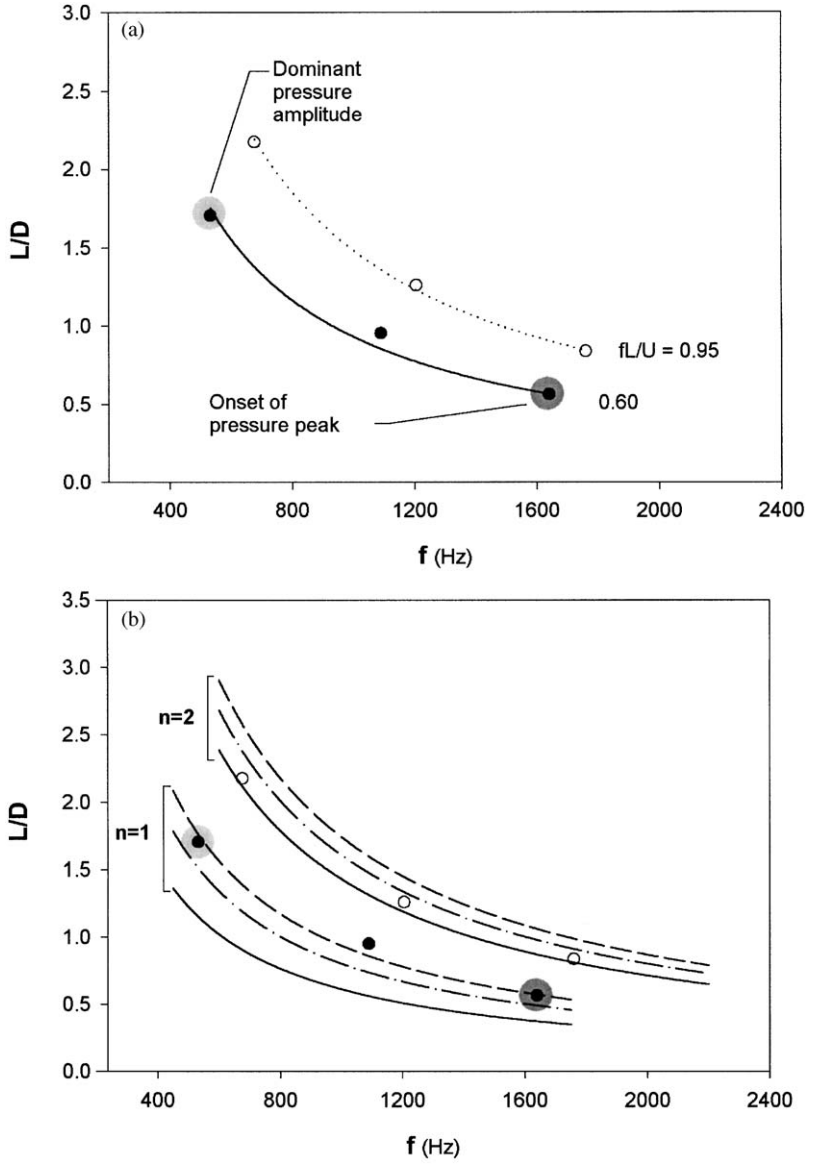

Fig. 14. Values of frequency corresponding to identifiable peaks in Fig. 8. Top plot (a) shows best fit through values of frequency and bottom plot (b) shows correlations for constant values of fL/U. (—) $fL/(0.86U) = 0.61(n-1/4)$; (- - -) $fL/(0.86U) = 0.61(n+1/6)$; (–·–·–) $fL/(0.86U) = 0.61n$. The designation dominant amplitude corresponds to the largest-amplitude peak, and onset of amplitude peak represents the occurrence of a sharply defined peak at a small value of cavity length.

6.1. Multiple modes scaled according to fD/U

In order to bring out the common features of the multiple mode behavior, data in Figs. 11–13, which represent the case of the long inlet pipe, are superposed on common axes in the plot of

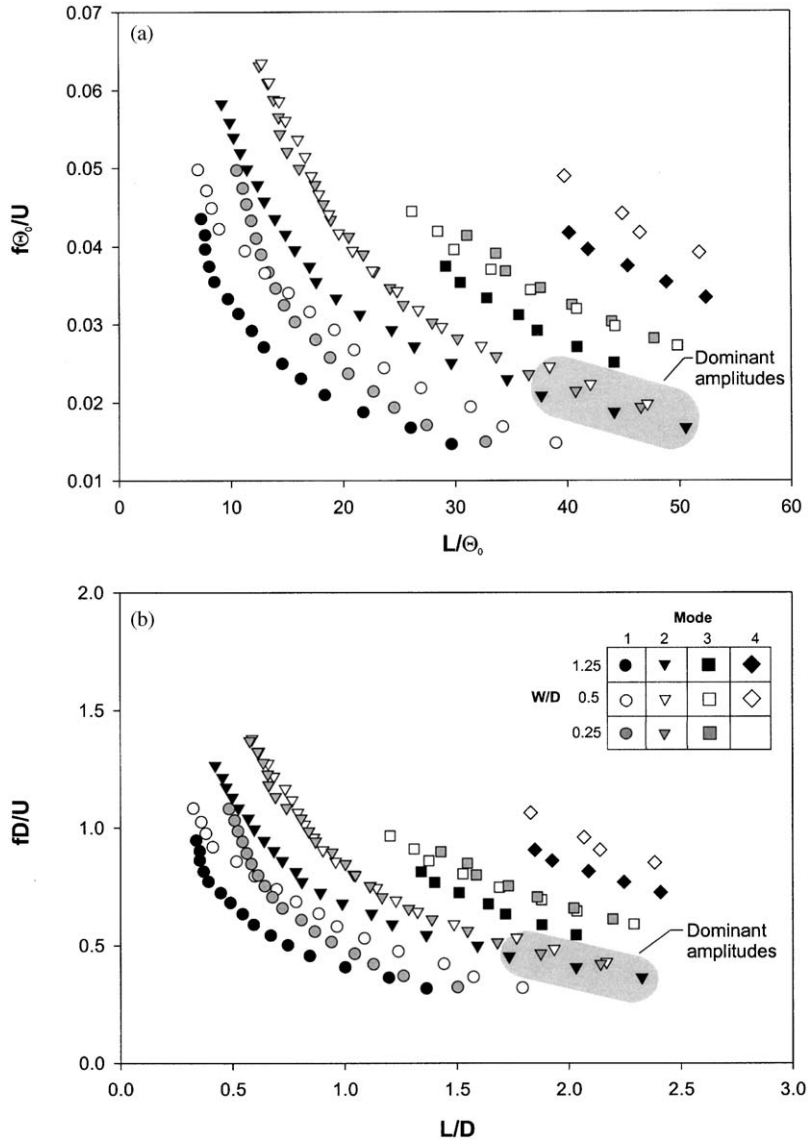

Fig. 15. Superposition of oscillation frequencies in each of the modes $n = 1-4$ at three different values of cavity depth W/D. (a) $f\Theta/U$, and (b) fD/U.

Fig. 15. These plots show scaling according to $f\theta_0/U$ and fD/U. In both plots, it is evident that the dimensionless frequencies for each of the modes $n = 1-4$ fall within narrow bands, i.e., the circular data points that represent mode 1 tend to cluster together. This collapse of the data occurs for the wide range of peak pressure amplitudes shown in the three-dimensional plots of Figs. 2–5. In these plots, it is evident that the amplitudes are substantially attenuated at smaller values of dimensionless depth W/D. Yet the frequencies corresponding to these peak amplitudes are close to those at larger values of W/D, where the peak amplitudes are much larger. This observation

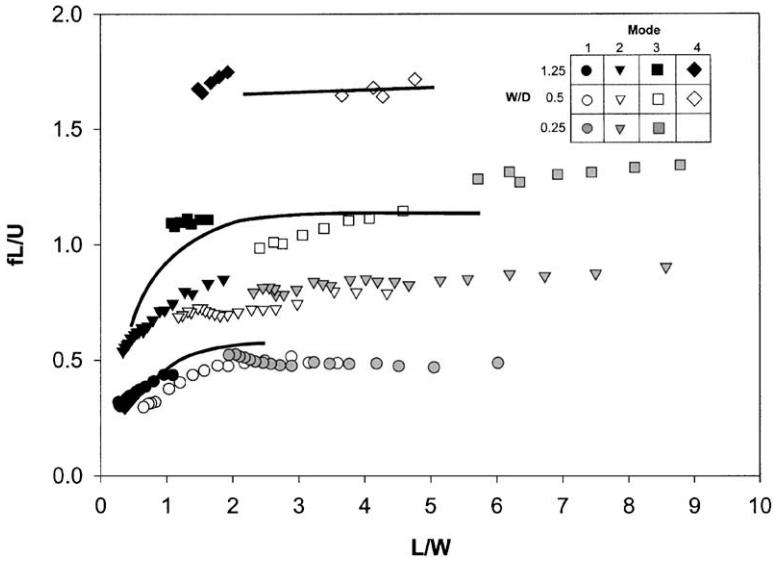

Fig. 16. Frequencies of oscillation normalized with respect to cavity length, i.e., fL/U versus ratio of cavity length depth, L/W for modes 1–4 at three different values of cavity depth $W/D = 0.25$, 0.5 and 1.25. (—) Correspond to a best fit through the data of Ethembabaoglu [29] corresponding to purely hydrodynamic oscillations in low-speed water flow.

suggests that the physical origin of the multiple modes is generally similar for all values of W/D; i.e., the same mechanism of shear layer instability most likely persists for all values of W/D.

6.2. Multiple modes scaled according to fL/U

Multiple modes have been represented by fL/U for purely hydrodynamic oscillations of flow past a cavity. The low-speed water experiments of Ethembabaoglu [29], without acoustic resonance, provide a basis for comparison with the present experiments involving acoustic resonant coupling. Fig. 16 shows data of the present experiments directly superposed on best-fit (solid) lines through the data of Ethembabaoglu [29]. It is evident that the general form of the multiple modes of the hydrodynamic oscillations is in overall accord with those of the present flow tone data. The major difference appears to be occurrence of a total of four distinct modes in the present investigation, as opposed to three in the data of Ethembabaoglu [29]. This distortion may be due to enhancement of additional mode(s) via occurrence of acoustic resonance. It should be kept in mind that the experiment of Ethembabaoglu [29] involved an external free-stream flow past a cavity, while the present situation corresponds to an initially turbulent jet flow through an axisymmetric cavity.

6.3. Multiple modes scaled according to fundamental β of oscillation

In the foregoing sections, the oscillation frequency of each of the multiple modes was scaled according to the pipe diameter D and the cavity length L. A different approach involves normalization with respect to the fundamental frequency component β, in a plot of $f\theta_0/U$ versus

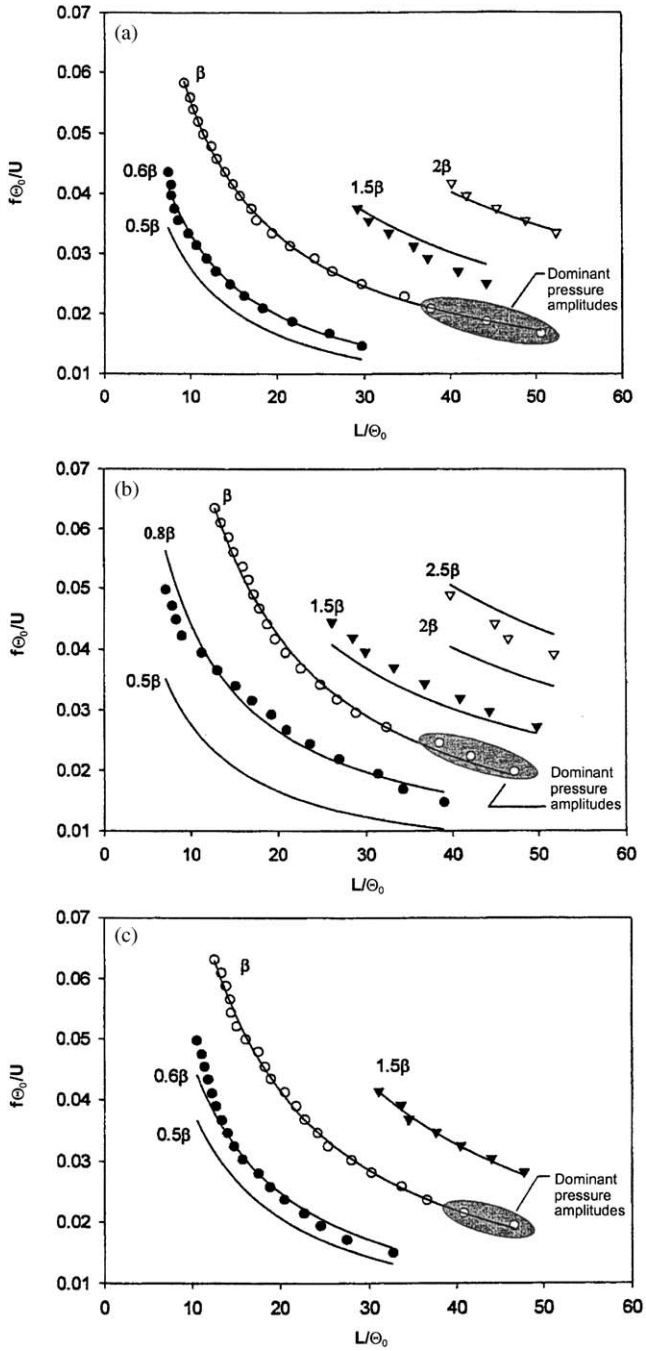

Fig. 17. Non-dimensionalized peak frequencies of pressure spectra as functions of non-dimensionalized cavity length. (a) $W/D = 1.25$, (b) $W/D = 0.5$, and (c) $W/D = 0.25$.

L/θ_0. For our present purposes, β is defined as the component that leads to the large-scale mode of vortex formation, and thereby the dominant pressure amplitude at large values of cavity length L.

The plots of Fig. 17 show non-dimensionalized peak frequencies of pressure spectra as functions of non-dimensional cavity length for three different values of cavity depth W, for the case of the long inlet pipe. The top plot corresponds to the deepest cavity, $W/D = 1.25$. At shorter values of cavity length, the fundamental frequency component β corresponding to the dominant pressure amplitudes coexists with a component at 0.6β. As the cavity length increases, the fundamental component β persists, in contrast to the 0.6β mode, which is not detectable for $L/\theta_0 > 30$. At $L/\theta_0 \cong 30$, a higher-order component appears at 1.5β. It is detectable for the range of values of L/θ_0 between 30 and 45. In addition to these modes, a 2β component exists for $L/\theta_0 > 30$.

The middle plot of Fig. 17 corresponds to the case of the intermediate value of cavity depth ($W/D = 0.5$). Similar to the previously described case of the deep cavity, three additional modes of shear layer oscillation coexist with the fundamental frequency component β. These modes correspond approximately to 0.8β, 1.5β, and 2.5β.

The consequence of a further decrease of the cavity depth ($W/D = 0.25$) is illustrated in the bottom plot of Fig. 17. Behavior of the oscillation modes in this case is generally similar to the one described for the case of the deepest cavity ($W/D = 1.25$), except for the fact that the highest frequency component 2β is not detectable for the case of $W/D = 0.25$.

Viewing together all plots of Fig. 17, it is evident that when the fundamental β is identified, the coexisting oscillation modes may occur at 0.6β, 0.8β, 1.5β, and 2.5β. The dominant amplitudes are at β, 0.8β and 0.6β. For purely hydrodynamic oscillations of a planar shear layer past a cavity, Knisely and Rockwell [33] similarly found well-defined low-frequency components at 0.8β and 0.6β, in addition to 0.4β and 0.2β. They related their occurrence to nonlinear interaction phenomena, as characterized by a bicoherence technique.

7. Predominant mode of oscillation: scaling according to stability concepts

Scaling of the frequency f of the self-excited oscillation using the diameter D or momentum thickness θ_0 allows links to be established to the inherent instability of the cavity shear layer. In the following, scaling based on instability concepts for the extreme cases of the large- and small-scale modes is addressed.

7.1. Scaling of large-scale mode

Oscillations that occur at relatively long cavity length allow full development of the large-scale, axisymmetric instability of the shear flow along the cavity. This instability is represented by the top schematic of Fig. 18. Blake [4] has correlated data from a wide variety of self-excited and forced (via a loudspeaker) axisymmetric jets in absence of a bounding cavity, and showed that the frequency of the large-scale mode lies in the range $0.3 \leqslant fD/U \leqslant 0.6$. The investigation of Rockwell et al. [8] showed that the dimensionless frequencies of the large-scale mode past an axisymmetric cavity lie in this range, irrespective of the thickness of the inflow boundary layer. At short values of cavity length L, however, the large-scale mode does not have the opportunity to develop, and it

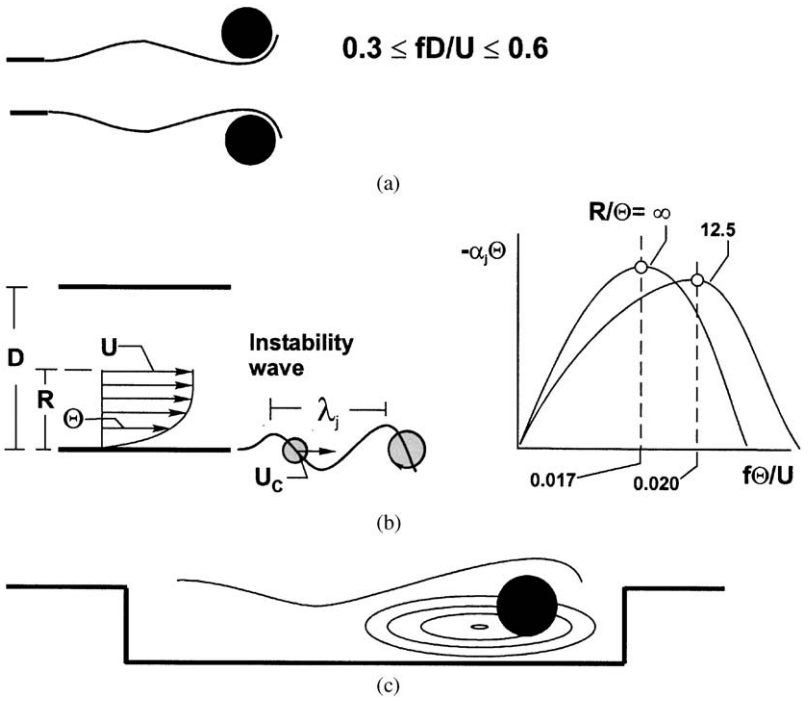

Fig. 18. Simplified representations of (a) fully evolved axisymmetric instability, (b) initial instability of a thin shear layer, and (c) global (absolute) instability.

is appropriate to consider a length scale based on the thickness of the inflow boundary layer, as described in the next section.

7.2. Scaling of small-scale mode

Oscillations at relatively short cavity length are defined as small-scale modes (Section 1.3). The basic features of a small-scale, convective-type instability are shown in the middle set of schematics of Fig. 18. Separation of the boundary layer gives rise to an instability wave of wavelength λ_i. Vortices move with a convective speed U_c in this separated layer. According to the instability analyses of Michalke [37,38], the values of amplification factor $-\alpha_i\theta_0$ versus dimensionless frequency $f\theta_0/U$ take the form shown in the schematic. For the limiting case where the radius R of the jet is infinitely large, relative to the momentum thickness θ_0, i.e., $R/\theta_0 = \infty$, the maximum value of $-\alpha_i\theta_0$ occurs at $f\theta_0/U = 0.017$. On the other hand, if $R/\theta_0 = 12.5$, the maximum value of $-\alpha_i\theta_0$ occurs at $f\theta_0/U = 0.020$. The value of $f\theta_0/U$ at which maximum amplification occurs is relatively insensitive to R/θ_0 in the range $12.5 \leqslant R/\theta_0 \leqslant \infty$. An important point of the schematic in Fig. 18 is that a relatively broad range of frequencies $f\theta_0/U$ has high values of amplification factor $-\alpha_i\theta_0$. This means that a range of frequencies of the unstable shear layer are susceptible to significant amplification. For the present case of the long inlet pipe, $R/\theta_0 = 10.86$, and for the case of the short inlet pipe, $R/\theta_0 = 31.25$.

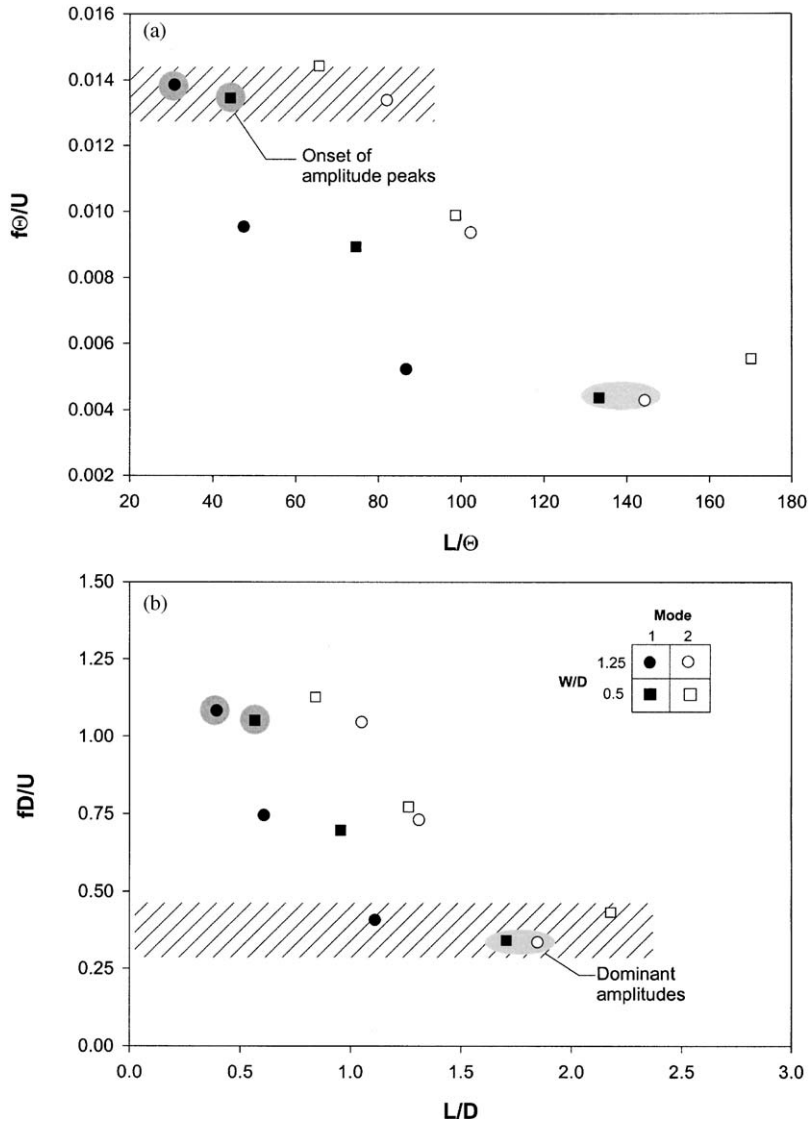

Fig. 19. Dimensionless frequencies of oscillation as a function of normalized length for different values of cavity depth. (a) $f\Theta/U$, and (b) fD/U.

Fig. 19 represents dimensionless frequencies for the case of the short inlet pipe. As shown in Fig. 19, the onset of an amplitude peak at short cavity length occurs at $f\theta_0/U \cong 0.014$; this value falls within the band of the most amplified dimensionless frequencies based on the inviscid stability theory of Michalke [37,38], as addressed in the foregoing paragraph and shown schematically in Fig. 18. On the other hand, the largest amplitude peak occurs at a much lower value $f\theta_0/U = 0.004$; this observation indicates that the thin shear layer mode, which occurs immediately downstream of the pipe exit, is not influential in determining the

dominant oscillation frequency at long cavity length. As shown in the bottom plot of Fig. 19, the dominant amplitude at $f\theta_0/U = 0.004$ corresponds to a value $fD/U$of approximately 0.35, which is in accord with the onset of the inherent, large-scale instability in the jet, as described in Section 5.1.2.

7.3. Extension of scaling of small-scale mode to large-scale mode

Inspection of zoomed-in views of individual spectra (not shown) allows further definition of the conditions for the onset of flow tones in both the small-scale and large-scale modes. For our present purposes, we define the onset of a pronounced tone as a peak in the spectrum that exceeds the nearest spectral peak by a factor of at least 20. A comparison is given in Tables 1 and 2. Table 1 corresponds to the onset of flow tones in the small-scale mode for the case of the short inlet pipe. These tones occur for relatively short cavity lengths. On the other hand, the data in Table 2 represent the onset of flow tones for the long inlet pipe, which occur in the large-scale mode.

Consider first Table 1, which represents cavity depths $W/D = 1.25$ and 0.5. The values of dimensionless frequency are both $f\theta_0/U = 0.013$, which is relatively close to the value predicted from linear stability theory, i.e., $f\theta_0/U = 0.017$. In comparison, note the value of fD/U= 1.02; it is well above the most unstable value ($0.3 \leqslant fD/U \leqslant 0.6$) for the large-scale mode of instability, which has not developed at these short values of cavity length. Also indicated are the values of cavity length at which this flow tone sets in. The dimensionless lengths are $L/\theta_0 = 24$ and 44. These values of L/θ_0 correspond to relatively small values of $L/D = 0.31$ and 0.56.

Regarding the onset of flow tones for the long inlet pipe represented in Table 2, spectra indicate that tones are not generated at short values of cavity length. Tones set in at relatively long lengths, i.e., $L/D = 2.1$ and 1.94, and the corresponding dimensionless frequency is $fD/U \cong 0.40$, which represents the onset of the large-scale mode. That is, these values of dimensionless frequency agree well with the column mode of instability of the jet. Finally, it should be noted that $f\theta_0/U = 0.018$ in Table 2 agrees reasonably well with the prediction from linear stability theory, i.e., $f\theta_0/U =$ 0.02, as described in Section 7.2 and illustrated in Fig. 18.

In summary, these observations indicate that the onset of the small-scale mode in the relatively thin shear layer at separation, represented in Table 1, occurs at values of dimensionless frequency in accord with linear stability theory. The onset of a so-called large-scale mode, indicated in Table 2, also can be compatible with the linear stability theory of Michalke [39], provided the relatively thick boundary layer at separation is accounted for in the analysis. In this case, the shear layer at separation is not thin relative to the pipe diameter, and a relatively long distance is required for

Table 1
Onset of flow tones of small-scale mode at relatively short cavity length (short inlet pipe)

W (in)	F (Hz)	$f\theta_0/U$	L (in)	L/θ_0
1.25	1,650	0.013	0.312	24
0.5	1,600	0.013	0.56	44

Cavity length varied; $U = 130$ ft/s.

Table 2
Onset of flow tones for large-scale mode at relatively long cavity length (long inlet pipe)

W (in)	f (Hz)	$f\theta_0/U$	L (in)	L/θ_0	L/D	fD/U
1.25	625	0.018	2.1	44	2.1	0.40
0.5	625	0.018	1.94	42	1.94	0.40

Cavity length varied; $U = 130\,\text{ft/s}$.

development of the instability. It is hypothesized that this is the reason why a flow tone cannot be generated at a relatively small value of L/D, unlike the case of the relatively thin shear layer at separation. This dimensionless frequency is compatible with the large-scale, column instability of the large-scale mode of vortex formation, which scales on diameter D of the pipe, i.e., jet. It should be noted, however, that scaling of the large-scale mode using diameter D is generally preferred because the large-scale mode always evolves to dimensionless frequencies $0.3 \lesssim fD/U \lesssim 0.6$ irrespective of the initial thickness of the shear layer.

8. Summary of principal features of flow tones as a function of cavity length at defined values of cavity depth

8.1. Variation of predominant frequency (IES) with cavity length

The variation of oscillation frequency with cavity length is bounded by two extreme modes. At large values of cavity length, the absolute value of frequency is relatively low. The appropriate length scale for characterizing the large-scale vortex formation is the diameter D of the jet, i.e., fD/U. At the other extreme, corresponding to short values of cavity length, the absolute frequency is relatively high, and the momentum thickness θ_0 of the separating boundary layer is the appropriate length scale for characterizing the initial instability, presumably associated with small-scale vortex formation. For the shortest values of cavity length, and thereby the highest frequencies, which exceed 1000 Hz, the values of the dimensionless frequencies lie approximately in the range $0.014 \lesssim f\theta_0/U \lesssim 0.025$.

An alternate form of scaling of the self-excited oscillation frequency involves the cavity length L, i.e., fL/U. In essence, this relationship is $fL/U = (U_c/U)(n + a)$, in which U_c is the phase speed, n is the mode (or stage) number, and a is an end correction. This dimensionless representation has been related to the effective phase speed of the instability wave or vortex system along the cavity and to the effective number of wavelengths along the mouth of the cavity. Although the models for fL/U provide valuable guidance, no single model provides a universal correlation of frequency f of the predominant mode versus cavity length L over a wide range of cavity depth W. For the deepest cavity, where the development of the separated shear layer is relatively unhindered by the finite depth of the cavity, the predominant frequency appears to undergo a transformation from an $n = 2$ to an $n = 1$ mode, as the cavity length L takes on successively smaller values. On the other hand, for shallower cavities, variation of f versus L closely follows the $n = 2$ mode.

8.2. Existence of multiple frequencies (modes) with variations of cavity length

At a given cavity length L, not only the predominant mode of oscillation (described in the preceding section), but also one or more additional modes are typically present. Different scaling representations have been employed, as summarized in the following.

8.2.1. Scaling according to fL/U versus L/D

Taken together, variation of all of these frequency components (or modes) with cavity length L exhibits a trend in accord with the $n = 1$, 2 and 3 modes of the relation $fL/U = (U_c/U)(n + a)$. No single value of a adequately predicts these multiple modes over a wide range of L/D for all cavity depths W/D.

8.2.2. Scaling according to fL/U versus L/W

In order to examine the role of the inherent hydrodynamic instability of the shear layer past the cavity, purely hydrodynamic data (in absence of acoustic resonance) based on low-speed experiments in water were compared with the present data. These experiments show that multiple modes occur in low-speed water flows, where acoustic resonance does not play a role. Broad agreement of the dimensionless frequencies fL/U as a function of L/W was obtained between the present data and the purely hydrodynamic data, except for existence of an additional mode in the present experiment. In other words, the effective source for the acoustic coupling phenomenon appears to exhibit a multiple mode behavior that persists in the presence of acoustic resonance. The hydrodynamic modes of the oscillating shear layer, i.e., source, must be compatible with those occurring during acoustic resonance. Of course, each of the multiple hydrodynamic modes may be distorted somewhat due to the necessity of lining up with the acoustic resonant modes of the pipe–cavity system.

In fact, another type of compatibility condition must also be satisfied. Flow tones appear to occur only when the even modes of the pipe–cavity system are excited. Independent experiments, not reported herein, demonstrated that acoustic resonance was possible only for even modes when the system was either excited with a loudspeaker or by a broadband turbulent boundary layer for the limiting case of cavity length $L = 0$.

8.2.3. Scaling according to $f\theta_0/U$ versus L/θ_0 and fD/U versus L/D

Since these multiple frequencies, or modes, occur for a wide range of cavity depth W, it is insightful to superpose values of dimensionless frequencies $f\theta_0/U$ and fD/U versus dimensionless cavity length L/θ_0 and L/D for all coexisting modes. This superposition shows that, in a broad sense, data for all values of W/D tend to collapse into an identifiable band for a given mode number $n = 1$, 2, 3, or 4. It is interesting that this type of collapse occurs even for relatively shallow cavities with small depth W/D, for which the peak amplitudes of the pressure fluctuations are relatively low and the corresponding spectral peaks are not sharply defined. This observation suggests that a consistent mode(s) of hydrodynamic instability tends to occur for all values of cavity depth W.

8.2.4. Scaling according to the predominant frequency β of oscillation

All of the aforementioned scaling of each of the multiple-mode components involves normalization using the length L or depth W of the cavity geometry, or thickness θ_0 of the

inflow boundary layer. A different approach involves identification of the frequency β of the fundamental mode, which is associated with the largest peak amplitude at sufficiently long cavity length. It has been demonstrated that the multiple mode components below β are remarkably in accord with 0.6β or 0.8β. These components, taken together with the β components, represent the largest amplitudes. Components 0.6β and 0.8β were shown to persist in the unstable shear layer past a planar cavity in absence of acoustic resonance, which suggests that they are due to a mechanism of hydrodynamic instability, which is present during acoustic resonant coupling. Furthermore, additional, lower-amplitude components in the present experiment satisfy $1.5\beta, 2\beta$.

8.2.5. *Jumps between modes of oscillation*

A further observation on the existence of multiple modes concerns the effects of spacing of the resonant acoustic modes of the pipeline–cavity system, i.e., whether they are relatively closely packed, or widely spaced. For the case where they are relatively widely spaced, which occurs for the short pipeline–cavity system, the predominant flow tone mode actually can jump from successively higher to lower modes as cavity length L is varied, even though a number of multiple modes are detectable. On the other hand, for the closely packed resonant modes, which occur for the long pipeline–cavity system, no such jumps occur.

8.3. *Limiting value of cavity length for onset of flow tones*

Flow tones are generated when the dimensionless length L of the cavity exceeds a critical value. For the data presented herein, this minimum length is in the range $25 \lesssim L/\theta_0 \lesssim 45$. From a physical standpoint, this minimum length criterion means that a sufficiently long distance is required for the instability to develop a significantly large amplitude, such that it can promote a self-excited flow tone. Direct comparison with previous experiments on flow tone generation is difficult, since detailed characterization of the inflow boundary layer was not undertaken. The data of Schachenmann and Rockwell [36], corresponding to the case of a long pipe terminated by an axisymmetric cavity with an orifice at its outlet, found minimum values of cavity length $L/\theta_0 = 10-75$. For the case of purely hydrodynamic oscillations in the absence of acoustic resonance, the onset of a detectable instability in the cavity shear layer was found to occur at a minimum $L/\theta_0 = 50$ in the investigation of Knisely and Rockwell [33]. Taken together, all of these observations indicate that a sufficient streamwise length is required in order for the instability to develop to a sufficiently mature form, such that it promotes the generation of a flow tone. Differences from experiment to experiment on the minimum value of L/θ_0 no doubt arise from different states of the inflow boundary layer, i.e., laminar versus turbulent and different values of damping of the acoustic resonator.

Acknowledgments

The authors acknowledge financial support through the Office of Naval Research, Grant N00014-98-1-0817, with supplemental support from the Office of Naval Research, Grant N00014-99-1-0581 (DURIP), and the Air Force Office of Scientific Research, Grant F49620-00-1-0009.

References

[1] D. Rockwell, E. Naudascher, Review—self-sustaining oscillations of flow past cavities, *Journal of Fluids Engineering* 100 (1978) 152–165.

[2] D. Rockwell, E. Naudascher, Self-sustained oscillations of impinging free-shear layers, *Annual Review of Fluid Mechanics* 11 (1979) 67–94.

[3] D. Rockwell, Oscillations of impinging shear layers, Invited Lecture, *20th Aerospace Sciences Meeting of AIAA*, January 1981, Orlando, FL; AIAA Paper 81-0047; also see *AIAA Journal* 21 (1983) 645–664.

[4] W.K. Blake, *Mechanics of Flow-Induced Sound and Vibration*, Vols. 1 and 2, Academic Press, New York, 1986.

[5] M.S. Howe, Edge, cavity and aperture tones at very low Mach numbers, *Journal of Fluid Mechanics* 330 (1997) 61–84.

[6] M.S. Howe, *Acoustics of Fluid–Structure Interaction*, Cambridge University Press, Cambridge, MA, 1998.

[7] D. Rockwell, Vortex–body interactions, *Annual Review of Fluid Mechanics* 30 (1998) 199–229 (Invited lecture).

[8] D. Rockwell, J.-C. Lin, P. Oshkai, M. Reiss, M. Pollack, Shallow cavity flow tone experiments: onset of locked-on states, *Journal of Fluids and Structures* 17 (2003) 381–414.

[9] N.H. Fletcher, Air flow and sound generation in musical wind instruments, *Annual Review of Fluid Mechanics* 11 (1979) 123–146.

[10] K. Hourigan, M.C. Welsh, M.C. Thompson, A.N. Stokes, Aerodynamic sources of acoustic resonance in a duct with baffles, *Journal of Fluids and Structures* 4 (1990) 345–370.

[11] A.K. Stoubos, C. Benocci, E. Palli, G.K. Stoubos, D. Olivari, Aerodynamically generated acoustic resonance in a pipe with annular flow restrictors, *Journal of Fluids and Structures* 13 (1999) 755–778.

[12] F.C. DeMetz, T.M. Farabee, Laminar and turbulent shear flow-induced resonances, AIAA Paper 77-1293, 1977.

[13] S.A. Elder, Self-excited depth-mode resonance for a wall-mounted cavity in turbulent flow, *Journal of the Acoustical Society of America* 64 (3) (1978) 877–890.

[14] S.A. Elder, T.M. Farabee, F.C. DeMetz, Mechanisms of flow-excited cavity tones at low Mach number, *Journal of the Acoustical Society of America* 72 (2) (1982) 532–549.

[15] P.A. Nelson, N.A. Halliwell, P.E. Doak, Fluid dynamics of a flow excited resonance. Part I: experiment, *Journal of Sound and Vibration* 78 (1) (1981) 15–38.

[16] P.A. Nelson, N.A. Halliwell, P.E. Doak, Fluid dynamics of a flow excited resonance. Part II: flow acoustic interaction. The dissipation of sound at an edge, *Journal of Sound and Vibration* 91 (1983) 375–402.

[17] M.L. Pollack, Flow-induced tones in side-branch pipe resonators, *Journal of the Acoustical Society of America* 7 (4) (1980) 1153–1156.

[18] J.C. Bruggeman, A. Hirschberg, M.E.H. van Dongen, A.P.J. Wijnands, J. Gorter, Flow induced pulsations in gas transport systems: analysis of the influence of closed side branches, *Journal of Fluids Engineering* 111 (1989) 484–491.

[19] J.C. Bruggeman, A. Hirschberg, M.E.H. van Dongen, A.P.J. Wijnands, J. Gorter, Self-sustained aero-acoustic pulsations in gas transport systems: experimental study of the influence of closed side branches, *Journal of Sound and Vibration* 150 (1991) 371–393.

[20] P.C. Kriesels, M.C.A.M. Peters, A. Hirschberg, A.P.J. Wijnands, A. Iafrati, G. Riccaradi, R. Piva, J.-C. Bruggemann, High amplitude vortex-induced pulsations in a gas transport system, *Journal of Sound and Vibration* 184 (2) (1995) 343–368.

[21] S. Ziada, E.T. Bühlman, Self-excited resonances of two-side-branches in close proximity, *Journal of Fluids and Structures* 6 (1992) 583–601.

[22] S. Ziada, S. Shine, Strouhal numbers of flow-excited acoustic resonance of closed side branches, *Journal of Fluids and Structures* 13 (1999) 127–142.

[23] P.O.A.L. Davies, Flow-acoustic coupling in ducts, *Journal of Sound and Vibration* 77 (2) (1981) 191–209.

[24] P.O.A.L. Davies, Piston engine intake and exhaust system design, *Journal of Sound and Vibration* 190 (1996) 677–712.

[25] P.O.A.L. Davies, Aeroacoustics and time varying systems, *Journal of Sound and Vibration* 190 (1996) 345–362.

[26] D. Rockwell, A. Schachenmann, Self-generation of organized waves in an impinging turbulent jet at low Mach numbers, *Journal of Fluid Mechanics* 117 (1982) 425–441.

[27] D. Rockwell, A. Schachenmann, The organized shear layer due to oscillations of a turbulent jet through an axisymmetric cavity, *Journal of Sound and Vibration* 87 (3) (1983) 371–382.
[28] D. Rockwell, H. Karadogan, Oscillations of an impinging turbulent jet: coherence characterization via conditional sampling, *Journal of Sound and Vibration* 83 (1) (1982) 111–124.
[29] S. Ethembabaoglu, *On the fluctuating flow characteristics in the vicinity of gate slots*, Division of Hydraulic Engineering, University of Trondheim, Norwegian Institute of Technology, 1973.
[30] V. Sahohia, Experimental and Analytical Investigation of Oscillations in Flows over Cavities, PhD Thesis, California Institute of Technology, 1975.
[31] V. Sarohia, Experimental investigation of oscillations in flows over shallow cavities, *AIAA Journal* 15 (1977) 984–991.
[32] D. Rockwell, C. Knisely, Vortex–edge interactions: mechanisms for generating low frequency components, *Physics of Fluids* 23 (2) (1980) 239–240.
[33] C. Knisely, D. Rockwell, Self-sustained low-frequency components in an impinging shear layer, *Journal of Fluid Mechanics* 116 (1982) 157–186.
[34] M. Gharib, A. Roshko, The effect of flow oscillations on cavity drag, *Journal of Fluid Mechanics* 177 (1987) 501–530.
[35] K. K. Ahuja, J. Mendoza, Effects of cavity dimensions, boundary layer and temperature on cavity noise with emphasis on benchmark dated to validate computational aeroacoustic codes, NASA Contractor Report: Final Report Contact NAS1-19061, Task 13, 1995.
[36] A. Schachenmann, D. Rockwell, Self-sustained oscillations of turbulent pipe flow terminated by an axisymmetric cavity, *Journal of Sound and Vibration* 73 (1) (1980) 61–72.
[37] A. Michalke, On spatially growing disturbances in an inviscid shear layer, *Journal of Fluid Mechanics* 23 (3) (1965) 521–544.
[38] A. Michalke, D. Küchemann, eds.), *The Instability of Free Shear Layers, Progress in Aerospace Sciences*, vol. 12, Pergamon Press, New York, 1972, pp. 213–239.
[39] A. Michalke, Instabilität eines kompressiblen runden freistrahls unter berücksichtigung des einflusses der strahlgrenzschichtdicke, *Zeitschrift für Flugwissenschaften* 19 (1971) 319.